A Precision UV-Wet Chemical Oxidation Dissolved Organic Carbon Analyzer

By

Max Liao

Under the Direction of Mark Haidekker and Aron Stubbins

Abstract:

This study is aimed at the development of a high-precision (sub-μMolar) dissolved organic carbon (DOC) analyzer for aquatic samples. The prototype analyzer uses ultraviolet and wet chemical oxidation (UV-WCO) aided with heat to oxidize DOC contents in samples. The oxidized DOC in the form of CO_2 is sparged from the solution at a defined flow rate and can be precisely determined through the use of a non-dispersive infrared (NDIR) gas analyzer. This prototype aims to improve on existing instruments by having sub-μM precision, near-continuous sample injection, and compatibility with analysis on board ships. It has potential applications for studies of DOC consumption and production by various mechanisms including but not limited to microbial respiration/carbon fixation, photochemical oxidation, and the mixing of water masses. The prototype was constructed and optimized to improve oxidation efficiency and precision. This prototype did not meet the sub-μM goal due to several factors affecting oxidation efficiency and signal stability. If the stability issues can be addressed and oxidation efficiency increased to 100% the desired precision could be achieved.

A Precision UV-Wet Chemical Oxidation Dissolved Organic Carbon Analyzer

By

Max Liao

B.S. Electrical Engineering, Georgia Institute of Technology, 2012

The Thesis submitted to the Graduate Faculty of The University of Georgia in Partial Fulfillment of the Requirements for the Degree

MASTER OF SCIENCE

Athens, Georgia

2017

A Precision UV-Wet Chemical Oxidation Dissolved Organic Carbon Analyzer

By

Max Liao

Major Professors: Mark Haidekker
Aron Stubbins

Committee: Patricia Medeiros
Javad Mohammadpour
Kun Yao

Electronic Version Approved:
Suzanne Barbour
Dean of the Graduate School
The University of Georgia
December 2017

Acknowledgements

I wish to express my sincere gratitude to Dr. Aron Stubbins for his guidance and patience through the last two years. I am very grateful to Dr. Mark Haidekker for his knowledge and enthusiasm during this project. To my committee, Dr. Patricia Mederios, Dr. Javad Mohammadpour, and Dr. Kun Yao, I thank you for giving me the opportunity despite the long distance. To the members of the Stubbins Lab: I wish to thank Sasha Wagner, Lixin Zhu, Christina Codden, Kevin Ryan, Ziming Fang, Leanne Powers, and the numerous interns for being such great colleagues and a wonderful team. I wish to send an appreciation to the University of Georgia for their graduate program and introducing me to all the friends that I have made here. To the Skidaway Institute of Oceanography: I have loved my stay here; the organization and the city of Savannah will stay as a part of me for the rest of life. Finally I would like to acknowledge my loving parents for keeping me going through this journey.

Contents

List of Figures viii

List of Tables ix

Table of Acronyms x

1 Introduction 1

1.1 Dissolved Organic Matter 1

1.2 DOC Definition and Importance 1

1.3 Methods of Measurement 2

1.4 Problems with Existing Methods of Measurement 3

1.5 Commercial Instruments 4

1.6 Removal of Background DIC 4

1.7 Oxidation 5

1.8 Extraction 9

1.9 CO_2 Measurement Techniques 11

2 Methods and Materials 14

2.1 Degassing 15

2.2 Syringe Pump 16

2.3 Oxidation Chamber 17

2.4 Extraction Chamber 20

2.5 Nafion Water Trap 23

2.6 LiCor 7000 CO_2/H_2O Analyzer 24

2.7 Computer Controls 26

2.8 Chemical Samples and Reagents 28

3 Results and Analysis **29**

3.1 Stability 29

3.2 Oxidation Efficiency 34

4 Discussion **44**

4.1 Improving Signal Stability 44

4.2 Improving Oxidation Efficiency 44

5 Conclusions **47**

References **48**

Appendices **55**

List of Figures

1 Flow Chart for General Process of Dissolved Organic Carbon Measurement - Dissolved organic carbon is isolated through filtration, acidification, and degassing before oxidation. The oxidated carbon dioxide is extracted in gaseous form with a carbon-free gas before being dried of water vapor and sent to a measurement device. 3

2 Dissolved Inorganic Carbon Species with Respect to pH 4

3 Membrane Inlet Technology - Carbon dioxide in the aqueous sample permeates through the membrane and is extracted with a stream of carbon-free air. 10

4 Sparging Process - Carbon dioxide in the aqueous sample is extracted with a stream of mass-flow controlled carbon-free air through bubbling. 11

5 Typical Non-Dispersive Infrared Analyzer - Gas is pumped into the sample chamber and exposed to an infrared light source. An optical filter eliminates wavelengths outside of the characteristic absorption wavelength for the gas and the amount of attenuation is measured by the detector. 13

6 Schematic of System: Purple path - Degas Mode where dissolved inorganic carbon is removed from the sample. Black path - Measurement Mode where dissolved organic carbon is oxidized, carbon dioxide is extracted through sparging, dried with Nafion tubing, and sent to the non-dispersive infrared analyzer. 14

7 Degassing Vessel Lid Designed for Dissolved Inorganic Carbon Removal . . 15

8 Degassing Vessel Photograph 16

9 UV Spectrum for GPH212T5VH Lamp 18

10 Reaction Chamber Diagram 19

11 Reaction Chamber Photograph 20
12 Sparging Vessel with Dimensions 21
13 Sparging Vessel Photograph 22
14 Nafion Dryer - The sample gas is dried as water vapor permeates through the interior walls of the Nafion tubing and is carried away by a drying gas. 23
15 Residence Time Examples for 2 mmol Dissolved Inorganic Carbon Standard at Gas Flow Rates of 2.5 and 5 mL per min 31
16 Stability Examples for 2 mmol Dissolved Inorganic Carbon Standard at Gas Flow Rates of 5 and 10 mL per min 32
17 Gaseous Bubbles - The pockets of O_2 gas generated in the UV/H_2O_2 oxidation process affect signal stability. 33
18 Dissolved Organic Carbon Stability Example with a 1000 μM Standard - Signal Fluctuation is Resultant from Effects of the Oxidation Process . . . 34
19 Optimal Hydrogen Peroxide Concentrations for 1000 μM Freshwater Dissolved Organic Carbon Standard 36
20 Example of 100% Dissolved Organic Carbon Oxidation with Freshwater . . 39
21 Dissolved Organic Carbon Oxidation Efficiency of 1000 μM Standards with Varying Salinities 40
22 Dissolved Organic Carbon Remaining after Oxidation of Dock Samples at Varying Irradiation Times 43

List of Tables

1 Quantities for Ideal Gas Volume Calculation - Temperature and pressure values for this calculation are provided the by LiCor non-dispersive infrared analyzer. 25

2 Serial Interface Commands for Syringe Pump Control 27

3 Extraction Efficiency in Sparging Vessel for a Liquid Flow Rate of 1 mL per min - Reported factors: ramp time to plateau, temperature of the gas stream recorded by the LiCor non-dispersive infrared analyzer, gas pressure recorded by the LiCor, carbon dioxide concentration observed by the LiCor, expected concentration of carbon dioxide based upon dissolved inorganic concentration and flow rate of the aqueous sample, and extraction efficiency at varying extraction gas flow rates. 30

4 Non-Dispersive Infrared Analyzer Values after Oxidation of 1000 μM Freshwater Dissolved Organic Carbon Standard with Varying Oxidant Concentrations 35

5 Non-Dispersive Infrared Analyzer Values of High Salinity (35 grams per L) Samples after Oxidation with Varying Oxidant Concentrations 36

6 Oxidation Efficiency of 1000 μM Dissolved Organic Carbon Standard with Temperature Control Off vs On 38

7 Oxidation Efficiency vs Salinity 40

8 Dissolved Organic Carbon Remaining after Oxidation of 100 μM Freshwater Standards and Dock Samples at Natural pH vs pH2 41

9 Dissolved Organic Carbon Remaining after Oxidation of Dock Samples at Varying pH Values 42

10 Oxidation Efficiency vs Irradiation Time 43

Table of Acronyms

Acronym	Definitions
DOC	Dissolved Organic Carbon
DOM	Dissolved Organic Matter
DIC	Dissolved Inorganic Carbon
POM	Particulate Organic Matter
TOC	Total Organic Carbon
HTC	High Temperature Combustion
WCO	Wet Chemical Oxidation
MFC	Mass Flow Controller
NDIR	Non-Dispersive Infrared
PI	Proportional-Integral
IC	Integrated Circuit
PWM	Pulse Width Modulator
μM	Micro Moles per Liter
ppm	Parts per Million

1 Introduction

1.1 Dissolved Organic Matter

Total organic matter in marine systems can be divided into two major fractions: dissolved and particulate. Dissolved organic matter (DOM) can be physically separated from particulate organic matter (POM) through filtration. Organic matter that passes through a 0.1 - 0.45 μm filter is classified as dissolved while the non-dissolved, POM remains on the filter.

DOM controls a quantitatively important fraction of the global carbon cycle as dissolved organic carbon (DOC). The store of DOC in the oceans is one of the largest reservoirs for carbon in the biosphere [1]. Quantification of this pool is necessary to elucidate its role in the mass balance of carbon in oceanic models [2], as well as carbon fluxes and the effects of climate fluctuations on the oceanic carbon cycle. DOC is an actively cycling and ecologically important portion of aquatic ecosystems and has become an important measurement in both saline and freshwater samples [3]. As the levels of anthropogenic carbon released into the atmosphere increase and modern fields of ocean systems studies become more extensive and interconnected, there is an increasing desire to quantify and elucidate the roles DOC plays in the carbon cycle [4].

1.2 DOC Definition and Importance

The heterogeneous nature and structural complexity of DOM causes its quantification to rely primarily on the measurement of DOC [5]. Carbon consists of about 50% of most organic molecules and can be isolated from inorganic carbon for measurement.

DOC concentration in marine systems varies with biological activity as well as anthropogenic sources. The DOC pool of the ocean carries significant importance as a sink in the

global carbon cycle. DOC is the largest pool (about 10^{18} g) of reduced carbon in the ocean - which is comparable to the total mass of CO_2 in the atmosphere or the amount stored in the terrestrial forests and soil [6]. Even small changes in the oceanic DOC pool could cause significant perturbations in the global carbon cycle for large time scales (i.e., 1000 to 10000 years) [7]. About half of the carbon released by the burning of fossil fuels remains in the atmosphere with the remainder sequestered by the oceans and the terrestrial biosphere [8].

Vertical export of DOM from the surface ocean to depths is critical in the oceanic carbon cycle [9]. Bacterial communities in natural waters use biologically labile DOM to support an important portion of ocean carbon production. Sinking biomass from the surface ocean drives respiration in these communities and helps maintain a strong vertical carbon gradient. Evidence has shown that DOC contains a significant portion of the organic carbon flux below photic layers in the ocean [10]. Precise and accurate measurements of DOC are beneficial in understanding the vertical mass balance of carbon in this cycle.

1.3 Methods of Measurement

Various methods are extant for the analysis of DOC in seawater. These methods as they have been trialed are presented in the following introductory sections. Section 2 includes more in depth descriptions of the methods applied and developed during thesis work. The technologies and problems inherent in the measurement of DOC have been documented [11; 12]. Presently, the most common method for DOC quantification involves the oxidation of organic carbon into CO_2 and subsequent gas analysis of the CO_2 concentration in gaseous phase through infrared (IR) absorption. This oxidation includes the following techniques:

- high-temperature combustion [13] whereby a sample is oxidized in an oven at high temperatures (e.g., 600°C)

- wet chemical oxidation [14; 15] whereby a sample is oxidized using a chemical oxidizer
- ultraviolet photo oxidation [16] whereby a sample is oxidized with ultraviolet irradiation

An overview of the general process for DOC measurement is shown in Figure 1. DOC is isolated through filtration, acidification, and degassing before oxidation. The CO_2 produced by oxidizing DOC is extracted in gaseous form with a carbon-free gas before being dried of water vapor and sent to a measurement device.

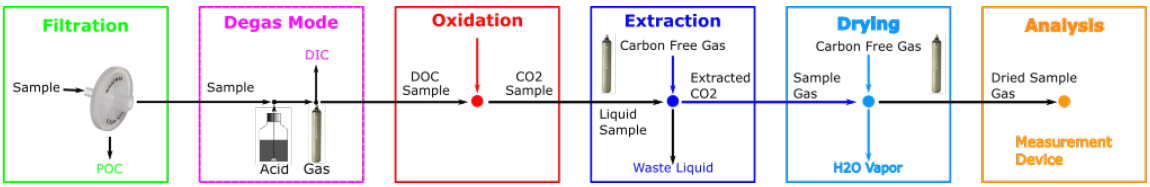

Figure 1: Flow Chart for General Process of Dissolved Organic Carbon Measurement - Dissolved organic carbon is isolated through filtration, acidification, and degassing before oxidation. The oxidated carbon dioxide is extracted in gaseous form with a carbon-free gas before being dried of water vapor and sent to a measurement device.

1.4 Problems with Existing Methods of Measurement

Much of the difficulty around the measurement of DOC is based on how it exists in seawater [11]. DOC in the oceans is a complex mixture of compounds with various molecular sizes, masses, and reactivities. Both halide interferences and the low amount of DOC in seawater are analytical obstacles [17]. Halides (mainly chlorine) interfere with oxidation by lowering the oxidative strength of chemical reagents [18; 19]. Despite the large total amount of carbon in the oceanic DOC pool, the concentrations are generally low with ~40 μM (0.5 ppm) in deep water and ~85 μM (1 ppm) in surface waters. Seawater contains dissolved inorganic carbon (DIC) concentrations (~2000 μM) at least an order of magnitude higher than their organic counterparts [20]. The large disparity between inorganic and organic

carbon molecules, low concentrations of DOC, and high salt contents of saltwater have been challenges to overcome for researchers seeking precise and artifact-free DOC analysis.

1.5 Commercial Instruments

Several commercial instruments exist on the market for the analysis of DOC. The precision of these instruments is typically in the μM range and is insufficient for analyzing small DOC differences caused by microbial respiration/carbon fixation [21], photochemical oxidation [22], and the mixing of water masses [23]. These systems are also dependent on system blank evaluations which can vary widely over time [24]. System blanks are reference samples made with carbon-free distilled water. A system with blank evaluations reduced to near-zero values could improve precision by an order of magnitude or greater.

1.6 Removal of Background DIC

After filtration, samples contain carbon in the form of both DIC or DOC. It is necessary to remove DIC from the sample due to its high concentration in seawater when compared with DOC [25].

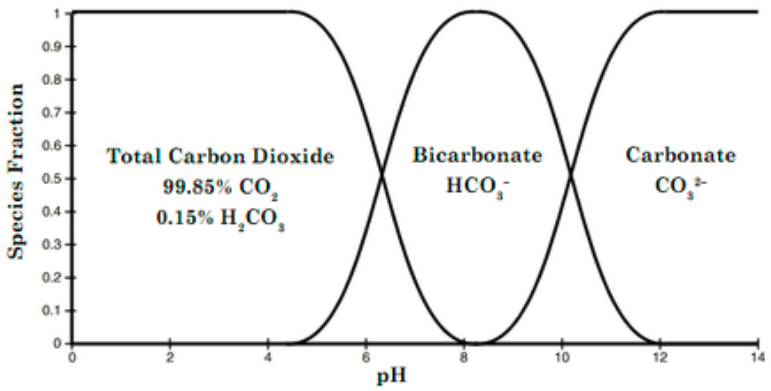

Figure 2: Dissolved Inorganic Carbon Species with Respect to pH

DIC removal is accomplished with acidification and purging [26]. Samples are brought to pH2 to convert DIC in the form of bicarbonate (HCO_3^-) and carbonate (CO_3^{-2}) ions into carbon dioxide (CO_2). The distribution of CO_2, HCO_3^-, and CO_3^{-2} along the pH spectrum can be seen in Figure 2 [27]. The DIC in the acidified sample is purged with a stream of carbon-free gas. The DOC remaining in the sample can then be oxidized for analysis.

1.7 Oxidation

The two most common processes for the conversion of DOC to DIC for analysis used in commercial devices are high temperature combustion (HTC) or wet chemical oxidation (WCO) [28].

High Temperature Combustion

The marine science community prefers the HTC technique because of its low sensitivity to salt, high oxidation efficiency, good accuracy and precision when properly blanked [3]. HTC systems rely on high temperature catalytic (e.g., platinum on aluminum oxide, cobalt oxide, copper oxide) combustion of the organic contents in the sample. HTC oxidation involves either dry combustion or direct aqueous injection [20].

In dry combustion, acidified samples are dried in a sealed tube and combusted, typically interacting with a catalyst, at over 600°C in a carbon-free high oxygen environment [29]. The organic carbon present in the sample is converted into CO_2 during the combustion. The subsequent gases are filtered for interferences. This purified gas is then analyzed with the use of an IR sensor.

In direct aqueous injection, a small amount of sample (e.g. 200 μL) is automatically injected into the oxidation column typically with a catalyst. The organic carbon present oxidizes into CO_2 before being dried, filtered, and purified for interferences (i.e., gas scrub-

bers). The amount of CO_2 is analyzed with the use of an IR device and then quantified by integrating the peak signal resulting from the combustion. Integration errors may occur and these HTC instruments typically perform multiple injections and report the average (e.g., 3-5 for the Shimadzu TOC-V_{CPH}).

These HTC instruments have a precision in the μM range (e.g., 50 μgrams per L for the Shimadzu TOC-V_{CPH}). There are significant sources of error associated with these analyzers in the form of sample injection, salt interference [26], memory effects [30], as well as system blank variability [31].

Wet Chemical Oxidation

Wet chemical oxidation makes use of oxidative chemicals (e.g., hydrogen peroxide (H_2O_2 [32]), ammonium persulfate ($(NH_4)_2S_2O_8$) [18]) to break down organics without the need for combustion. The oxidative power of these chemicals can be enhanced with a combination of UV radiation and heat to convert organic carbon into CO_2 [17]. This method offers a way to oxidize samples with high sensitivity, but current methods are not able to quantitatively convert DOC to DIC and are therefore not suitable for the quantification of DOC in seawater.

Ultraviolet Radiation

Ultra violet (UV) radiation is a form of electromagnetic radiation in the spectrum between visible light and X-rays (λ : 10-400 nm). When molecules are exposed to this form of radiation, the energy transmitted can be strong enough to ionize atoms and break chemical bonds. The extent of the energy absorbed is dependent on the wavelength of the radiation. Lower wavelengths provide greater radiated energy but can cause side effects (e.g., formation of ozone).

Photo oxidation is the oxidation of organics with the use of an electromagnetic source. UV irradiation of samples leads to the photo oxidation of DOC to CO_2 [33]. The wavelengths used for this process are typically in the UV-C range (λ : 100-280 nm). The energy produced at these wavelengths promotes the formation of free radicals such as hydroxyl (OH) which drives the oxidation process [34]. The oxidized CO_2 can subsequently be separated from the aqueous sample and sent to the analyzer with carbon-free gas.

Introducing intense low to medium pressure UV lamps during the oxidation stage promotes a high oxidation efficiency [35]. UV-C "germicidal" light (200-280 nm) has been used as an effective method for disinfecting water [36]. In a comparison made between UV-C light at a wavelength of 254 nm versus a combination of 254 and 185 nm, the combination led to more efficient degradation of the organics [16]. This is due to the higher energy levels provided at shorter wavelengths which generate more free radicals causing more efficient decomposition of refractory compounds [37]. It is assumed that organic molecules are affected by the long wave radiation (254 nm) mainly in the UV-active areas of the molecule while the short wave radiation (185 nm) causes OH radicals to form [38].

Combined UV-Wet Chemical Oxidation

The power of ultraviolet photo oxidation can be enhanced with the addition of a chemical oxidant. The ultraviolet/hydrogen peroxide (UV/H_2O_2) advanced oxidation process (AOP) has been extensively researched for the oxidation of organic contaminants [39; 40], pesticides, herbicides [41], and taste and odor compounds [42]. Continuous flow systems based on UV and WCO have allowed automated quantification of DOC in seawater in sub-ppm ranges [43].

The combination of UV and H_2O_2 creates a homogeneous light-driven oxidation which produces OH free-radicals through direct photolysis of H_2O_2 under UV radiation [44]. This can effectively oxidize DOC through mineralization. H_2O_2 has strong molar extinction coefficients (i.e., greater than 1.0 (1 per mol per cm)) below wavelengths of 300 nm with coefficients reaching values greater than 100 (1 per mol per cm) at wavelengths below 200 nm [45]. Due to these absorption characteristics, the reaction cells must be specially designed for UV irradiation at the utilized wavelengths.

H_2O_2 can be considered an effective OH radical scavenger. However, OH radicals react with organic molecules at rates roughly two orders of magnitude larger [46]. Its behavior under UV irradiation can be summarized by the following reactions [47; 48]:

$$H_2O + h\nu \longrightarrow 2\,OH \tag{1}$$

$$OH + H_2O_2 \longrightarrow HO_2 + H_2O \tag{2}$$

$$H_2O_2 + HO_2 \longrightarrow OH + H_2O + O_2 \tag{3}$$

$$2\,OH \longrightarrow H_2O_2 \tag{4}$$

$$2\,HO_2 \longrightarrow H_2O_2 + O_2 \tag{5}$$

$$OH + HO_2 \longrightarrow H_2O + O_2 \tag{6}$$

Due to its dependence on the UV source, the rate limiting reaction (equation 1) from these equations operates at a much slower rate. There exists an optimal H_2O_2 concentration for oxidation. Less than optimal oxidant concentrations result in dropping CO_2 signals due to the insufficient amount of H_2O_2 required for full oxidation. A too high concentration of H_2O_2 would result in reactions with OH radicals leading to the formation of hydroperoxyl,

HO_2 (equation 2). This implies that excessive H_2O_2 increases the operating cost, reduces the oxidation rate of organics, and also leaves residual H_2O_2 in the treated water [32].

OH radicals are effective in destroying organic molecules because of their electrophile reactivity. This characteristic causes them to react rapidly and nonselectively when in proximity to nearly all electron-rich organics. Once these free radicals are generated, they attack organic matter by hydrogen abstraction (equation 7), radical addition (equation 8), and electron transfer (equation 9) [49]. In the following equations OM represents the reacting organic compound:

$$\mathrm{OM} + \mathrm{OH} \longrightarrow \mathrm{OM\ Radical} + \mathrm{H_2O} \tag{7}$$

$$\mathrm{OM} + \mathrm{OH} \longrightarrow \mathrm{OM/OH} \tag{8}$$

$$\mathrm{OM^n} + \mathrm{OH} \longrightarrow \mathrm{OM^{n-1}} + \mathrm{OH^-} \tag{9}$$

Thermochemical UV-Oxidation

Also known as heated UV-WCO, this method utilizes the photo-chemical oxidative formation of free radicals in the UV-WCO process with the addition of elevated temperature. Heat enhances oxidation efficiency by magnifying the oxidizing power of the photo-chemical reactions and creating more free radicals (equation 1) [50]. To maintain precision and prevent any volume losses in the sample, the temperature of the system must be held below boiling (100° C).

1.8 Extraction

After oxidation the oxidated CO_2 must be separated from the liquid sample for analysis. The acidified sample at pH2 allows CO_2 to separate from the solution. Removal of CO_2

from the solution occurs inside an extraction cell with a stream of mass-flow controlled carbon-free air. This stream of gas is then filtered and dried before being sent to the analyzer. Possible methods for the extraction cell include membrane inlet technology or a sparging vessel.

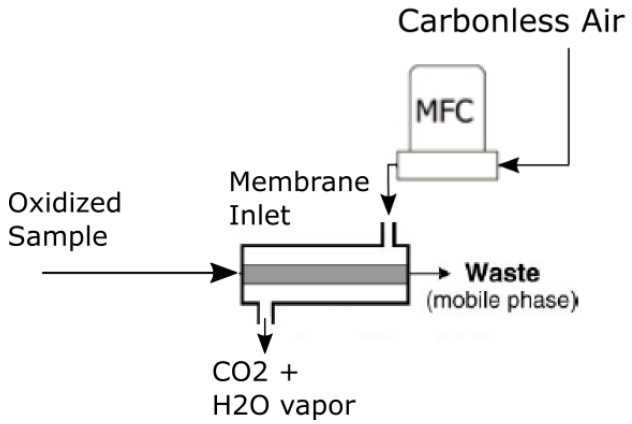

Figure 3: Membrane Inlet Technology - Carbon dioxide in the aqueous sample permeates through the membrane and is extracted with a stream of carbon-free air.

Membrane inlet technology allows for the separation of gases from liquid samples through permeable membranes. Polydimethylsilioxane (PDMS) is a silicon based organic polymer that can be used to separate gas species [51]. PDMS is highly permeable for CO_2 but dense enough that liquids cannot transfer through. These membranes operate by introducing a stream of gas flowing counter to the liquid sample which removes CO_2 that permeates out of the membrane as shown in Figure 3. Selective permeation of gases through this membrane is dependent on the solubility and rate of diffusion of the gas species as well as the thickness of the membrane.

Another method of CO_2 extraction involves sparging. A sparging vessel is used to strip CO_2 from the liquid sample as seen in Figure 4. The oxidized sample is introduced to a vessel with a steady stream of carrier gas. This carbon-free gas creates bubbles throughout the sample and releases the CO_2 to be sent to the analyzer.

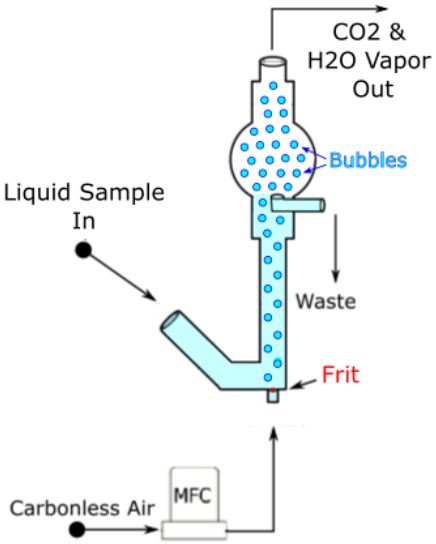

Figure 4: Sparging Process -
Carbon dioxide in the aqueous sample is extracted with a stream of mass-flow controlled carbon-free air through bubbling.

1.9 CO_2 Measurement Techniques

The system makes use of a continuous reaction technique. The sample is continuously oxidized over extended periods of time. The CO_2 produced from oxidation of DOC is sparged from the sample with a steady flow rate ideally producing a stable signal plateau at the analyzer. This technique provides a signal with a higher level of precision due to the large number of data points and eliminates errors associated with peak integration used in most HTC systems. For the analysis of DIC, this technique has been demonstrated to have a precision of about 0.05% and be able to discern differences of less than 0.1 μM [52].

A precise quantification of CO_2 is critical to the operation of the instrument. Various sensors are reported in the literature for the analysis and measurement of CO_2 [53; 54]. These technologies can be categorized by the two most common technologies: electrochemical gas and non-dispersive infrared (NDIR) sensors.

Chemical Gas Sensors

Electrochemical gas sensors operate by diffusing a gas through a permeable membrane to an electrolyte where it is oxidized or reduced before reaching an electrode where it is sensed [55; 56]. This reaction produces current that can be used by an external circuit to determine the concentrations of various species in the gas. The sensor analyzes current before and after oxidation to determine the difference in CO_2.

Chemical gas sensors have principal advantages in their low energy consumption and small hardware sizes. They have disadvantages with drift effects, shorter lifetimes, and lower durability when compared with NDIR sensors [57].

Non-Dispersive Infrared Sensors

NDIR sensors are spectroscopic devices used to analyze the characteristic absorption of gas species. Analytical techniques for the precise determination of CO_2 have been documented using an NDIR sensor [58]. Measurements made by the sensor are based off the Beer - Lambert law. This law relates light attenuation through a sample with its chemical properties. At the correct wavelength, the amount of CO_2 in the gas sample can be determined from the attenuation of the signal from the IR source indicated at the IR detector.

The two main types of IR detectors are thermal and photonic. Thermal sensors measure changes in temperature based on resistance [59], thermoelectric [60], or pyroelectric [61] effects of the IR signal. Photonic sensors are semiconductor devices that experience electronic excitation when exposed to IR photons and can have faster response times and sensitivity compared to thermal sensors [62]. H_2O vapor can interfere with an NDIR analyzer's response to CO_2 at the detector. Dehumidified samples are preferred for analysis in IR wavelengths [63]. Relevant sensing wavelengths for CO_2 are 4.26 μm, 2.7 μm [64], and

$\sim$13 μm. The relevant sensing wavelengths for H_2O vapor are 1.3 - 1.4 μm, 1.8 μm, 1.94 μm, and 2.75 - 2.85 μm [65].

A typical NDIR device shown in Figure 5 contains an IR source, an optical filter, a sample chamber, and IR detector. The gas to be measured is pumped into the sample chamber. The IR light passes through the sample chamber towards the IR detector. An optical filter eliminates the wavelengths outside of the characteristic absorption wavelength for the gas. The amount of attenuation in these wavelengths is measured by the detector. This value can be compared with a reference gas of known concentration to provide an accurate measurement of the sample.

Analysis with NDIR devices offers a practical method of measurement with little interference from drift effects [66]. These devices are vibration insensitive and can be applicable for analysis at sea [67]. An NDIR gas analyzer is used in this system for the determination of CO_2 produced from the oxidation of DOC.

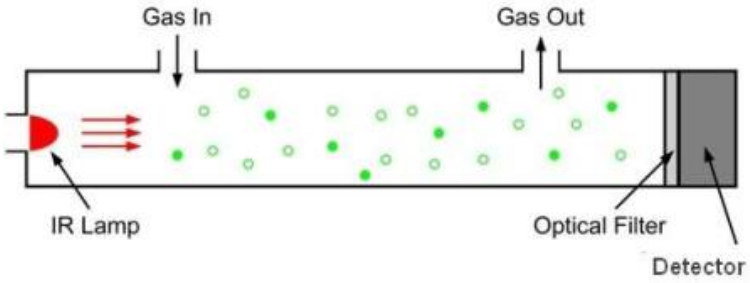

Figure 5: Typical Non-Dispersive Infrared Analyzer - Gas is pumped into the sample chamber and exposed to an infrared light source. An optical filter eliminates wavelengths outside of the characteristic absorption wavelength for the gas and the amount of attenuation is measured by the detector.

2 Methods and Materials

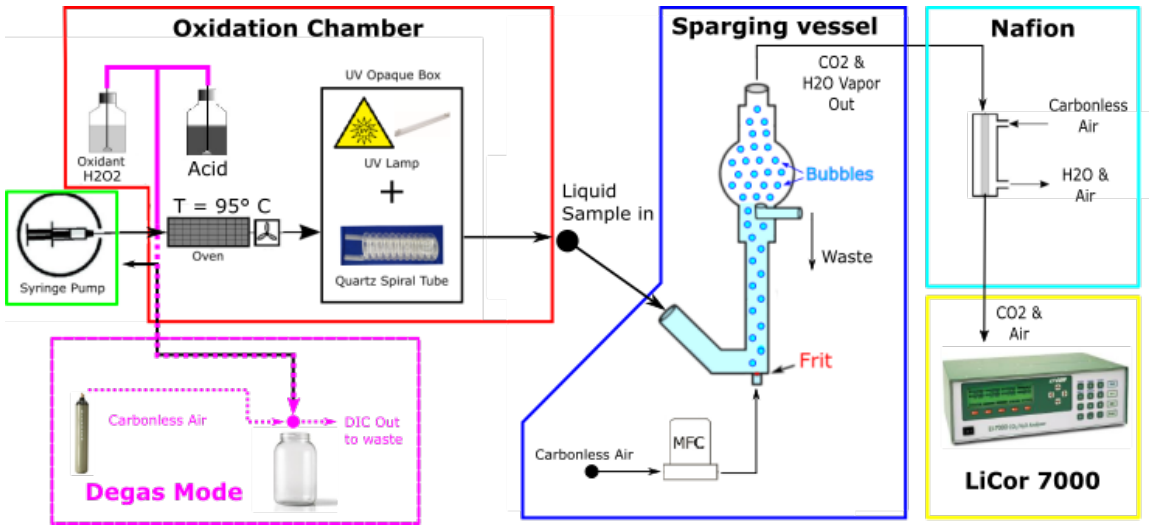

Figure 6: Schematic of System:
Purple path - Degas Mode where dissolved inorganic carbon is removed from the sample.
Black path - Measurement Mode where dissolved organic carbon is oxidized, carbon dioxide is extracted through sparging, dried with Nafion tubing, and sent to the non-dispersive infrared analyzer.

A prototype system for UV-WCO DOC analysis was constructed and attempts were made to optimize the system for high salinity samples. The goals for the system include 100% oxidation of DOC for marine samples as well as signal stability and precision in the sub-μM range. For this purpose we decided to use the following design including low flow sample injection, UV-WCO, and a sparging vessel for extracting oxidized CO_2. Figure 6 shows the DOC analysis system in its entirety with the purple path showing degas mode and the black path displaying measurement mode.

2.1 Degassing

A degassing mode is implemented in the system to allow the offline removal of DIC before the analysis of DOC. A modified jar with two luer lock attachments on the lid is filled with sample that is pre-acidified to pH2. These luer locks have close valves which can be manually changed to switch between degassing and measurement modes as shown in Figure 7. One of these is connected to the syringe pump and the other is attached to a stream of purge gas. The close valves ensure that the gas and liquid flows can be controlled without interference. The lid has a small hole to allow the release of gases from the sample. When the system is placed into degassing mode, the purge gas enters one of the luer locks and is carried by a tube to the bottom of the jar where a bubbler is attached. The purge gas bubbles through the sample and releases DIC from the solution in the form of CO_2. A photograph of the jar is shown in Figure 8.

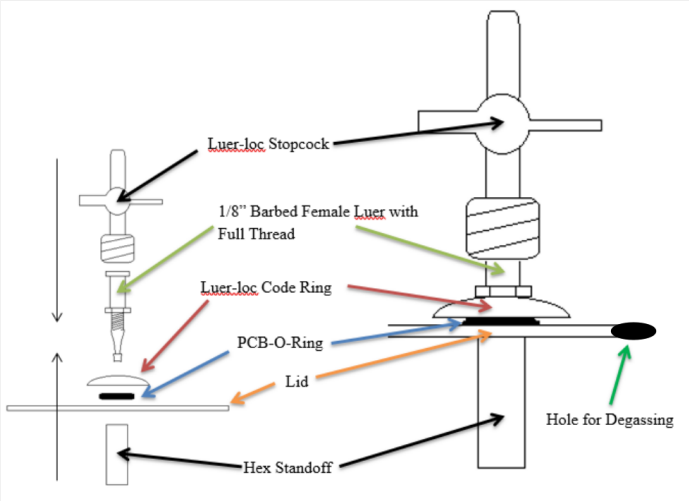

Figure 7: Degassing Vessel Lid Designed for Dissolved Inorganic Carbon Removal

When degassing is complete the valves can be switched and the system proceeds to measurement mode. The DIC-free sample is extracted from the degassing vessel and flows

into the syringe pump through the other luer lock connector. A three-way valve controls the flow of sample from the degassing vessel to the pump and from the syringe to the rest of the system.

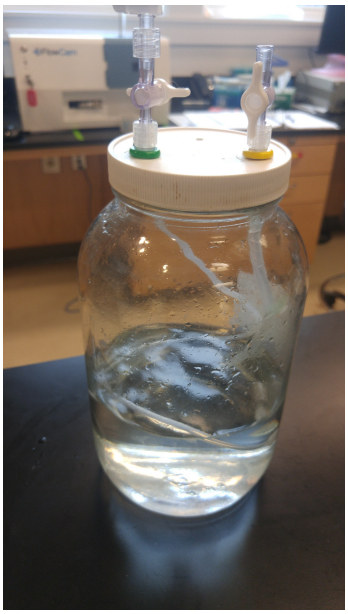

Figure 8: Degassing Vessel Photograph

2.2 Syringe Pump

After degassing, the system proceeds to measurement mode where the sample is introduced into the system via a custom built syringe pump.

This syringe pump was constructed with the goal of injecting sample at a steady and low flow rate ($\leq$1 mL per min). The pump includes mounting for the syringes, a stepper motor attached to a lead screw to drive the syringe flow, a linear stage with positional feedback to provide controlled plunger motion, as well as the electronics.

The syringe pump is powered by a stepper motor (Anaheim Automation 23AV102). The motor has a lead screw with a pitch size of 0.05 inches. This pitch size allows for small

movements required to obtain low flow rates for the sample. The resolution on these flow rates can be further enhanced with the application of half stepping or microstepping. A table providing the step sequences for each stepping resolution is in Appendix A.

The motor driver is provided by a dual H-bridge (UDN2998W). This low-cost integrated circuit (IC) provides the controllable current necessary to drive the motor. The H-Bridge is powered with 12V as the recommended minimum voltage for the IC is 10V. The motor coils are recommended to be driven at 5V so pulse width modulator (PWM) signals are employed to bring the H-bridge outputs down to the desired voltage. PWM frequencies are kept an order of magnitude faster than the motor step frequencies and can be modified in the software.

The glass syringes (Cadence-G5331) have a graduated volume of 150 mL and are designed for dissolved gas analysis. These syringes were chosen for their large size and the smoother flow rates glass provides compared to their plastic counterparts. Two of these syringes are mounted side by side on a sheet of aluminum with 3D printed plastic seen in Appendix B. The plungers are similarly attached on top of a linear stage (Daedel MX80L). The linear stage has near friction-less motion and provides feedback for its movement.

2.3 Oxidation Chamber

The syringe pump introduces sample to the reaction chamber where oxidation is accomplished with a combination of heat, photo and wet-chemical oxidation.

The heating element is provided by a length of resistive wire (Nichrome: 1 mm diameter, 1.35 Ω/m) attached to the outside of a cylindrical piece of copper foil (1 mm thick and 150 mm long). The wire is coated with thermally conductive epoxy to provide electrical insulation while maintaining heat transfer. The wire is held into place around the copper foil with three hose clamps - these clamps also help keep the shape of the copper sleeve.

The power supplied to the heating wire is controlled through a feedback system which includes a modified proportional-integral (PI) controller, T-type precision thermocouple sensor with a digital converter (MAX31856), and mosfet driver (50N06).

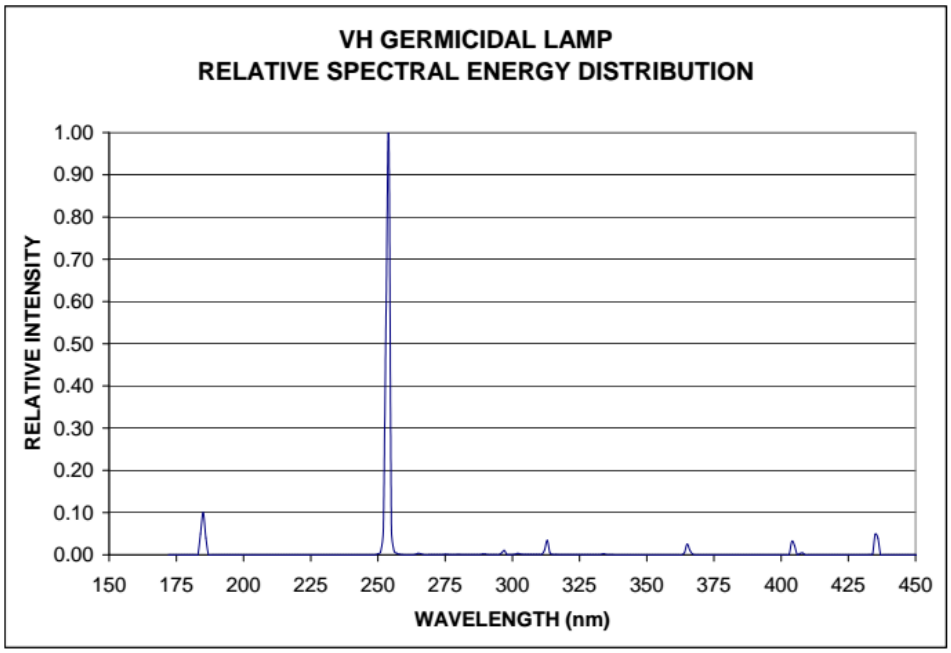

Figure 9: UV Spectrum for GPH212T5VH Lamp

photo oxidation occurs with sample injection through a custom UV-transparent quartz coil surrounding a UV lamp (GPH212T5VH). This low-cost (∼$25) 10W lamp was purchased from Amazon and is encased inside a quartz tube to allow UV spectral outputs with peaks at 185 and 254 nm - two bands ideal for the oxidation of DOC [68].

This lamp outputs 27 μW per cm^2 at 254 nm and its spectral output can be seen in Figure 9. It also produces a significant amount of heat, thereby reducing the amount of power required from the heating wire. This heating effect is enhanced by insulation covering the copper heating sleeve. The lamp without the temperature controller is capable of generating temperatures reaching and exceeding the set point of 95° C if given enough

time. However this temperature drops when room temperature samples are introduced to the reaction chamber. This drop is dependent on the temperature and flow rate of the sample. The modified PI controller provides enhanced heating speeds and maintains a stable temperature while the system is in measurement mode.

The quartz coil is designed to maximize UV exposure from the lamp to the sample through geometry and UV transparency. The resulting design has a spiral geometry with an inner diameter of 1.0 mm with a total length of 1130.4 mm leading to a volume of around 0.888 mL. The outer diameter of the coil is ~1/8 inch to allow for easy Swagelok plumbing. The custom design was purchased from Donghai County Teng Hui Quartz Material Co Ltd.

The chemical oxidant used was a 30% w/w H_2O_2 solution with a stabilizer (i.e., 0.5 ppm stannate-containing compounds and 1 ppm phosphorus-containing compounds). An optimal concentration of this oxidant is mixed with the pre-acidified sample prior to de-gassing mode. The degassing process helps distribute the oxidant evenly in the solution. The optimal oxidant concentration is discovered through empirical testing as described in Section 3.2.1.

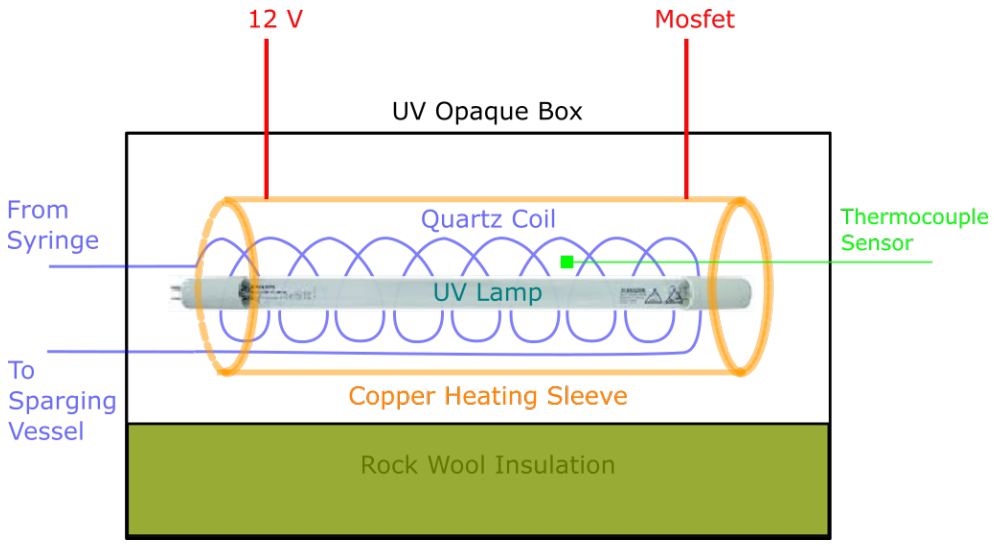

Figure 10: Reaction Chamber Diagram

Figure 11: Reaction Chamber Photograph

The oxidation reaction occurs inside an UV opaque irradiation box designed to prevent light leakage. The bottom and sides of the box are insulated with rock wool to maintain temperature. The UV lamp, quartz coil, heating element, and insulation are placed inside the reaction chamber as shown in Figures 10 and 11.

2.4 Extraction Chamber

Two designs for a CO_2 extraction cell were examined for this system. The methods examined were membrane inlet technology and a sparging vessel. These methods were compared with respect to their extraction efficiency for CO_2 from the oxidized liquid sample.

Membrane Inlet Silicone

The first design made for CO_2 extraction made use of a porous membrane inlet design. The PDMS membrane tested (PermSelect PDMSXA-10) is an extraction module with typical liquid flow rates in the low ranges required by the system (1 - 10 mL per min).

Sparging Vessel

The second design used for the extraction of oxidized CO_2 from the liquid sample is a glass sparging vessel. The vessel dimensions are kept small to reduce the sample volume (∼1.7 mL) and therefore the residence time of the sample for full degassing as seen in Figures 12 and 13.

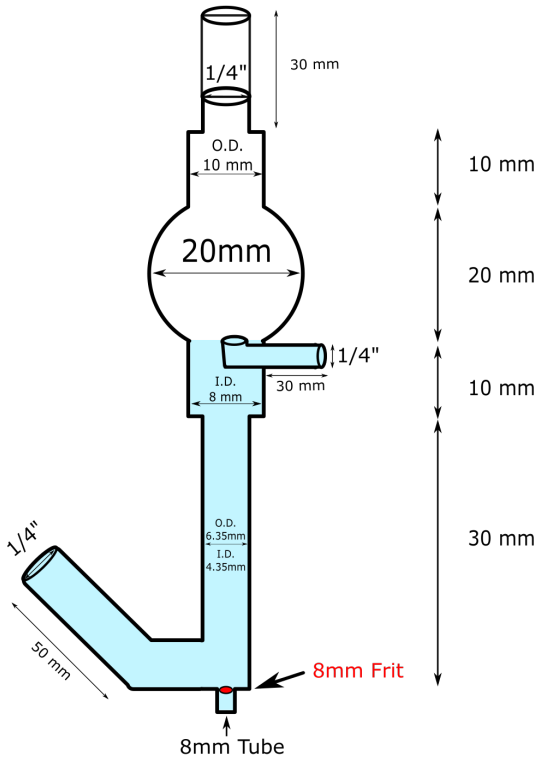

Figure 12: Sparging Vessel with Dimensions

The syringe pump introduces the sample through the reaction chamber and into the bottom of the vessel above a frit (8 mm Type-E). Carbon-free carrier gas is introduced by a low-flow mass flow controller (MFC) (Omega GR116) through the frit. This MFC can control the carrier gas flow rate between 1-10 mL per min (± 1%).

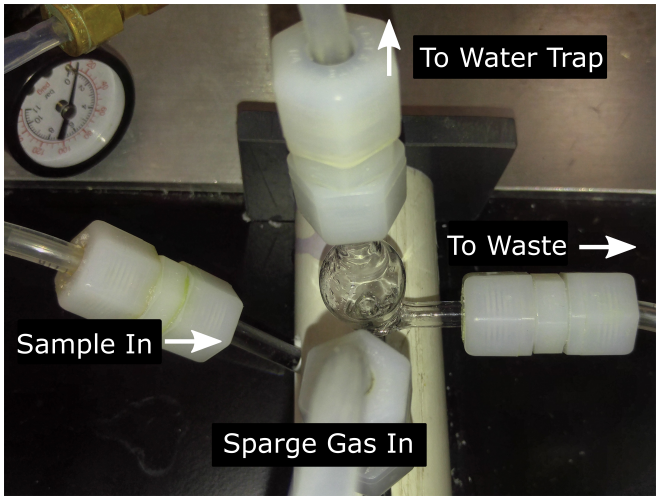

Figure 13: Sparging Vessel Photograph

The high-porosity frit causes the carrier gas to bubble through and release the CO_2 from the sample. The carrier gas and CO_2 from the sample outflow from the top of the vessel towards a water trap. The stripped liquid sample is removed out the side of the vessel with a peristaltic pump. These methods have been documented with a sparging vessel for the analysis of DIC [52].

A pure air generator or a tank of compressed air can be used to provide carbon-free air. Attempts were made using a zero-gas generator (AirGen TOC AirGen GC). The generator produced gas in a cyclical manner and made use of an inconsistent gas source - a standard 150 psi air compressor. The cyclical manner in which it provided carbon-free air created pressure variations which contradicted the system demands for stable flow rates and caused fluctuations in the MFC flow rates.

Zero-grade air is a synthetic gas commonly used for the calibration of environmental monitoring equipment such as the LiCor 7000 CO_2 analyzer used in this system. Zero-grade air from a tank is preferred in the sparging process for its carbon neutrality and pressure stability.

2.5 Nafion Water Trap

Gas analysis with the NDIR analyzer requires a clean and dry sample for precise results due to the contaminating effects of H_2O and particulates on IR detection. Particulates and water vapor extracted alongside CO_2 from the sample must be removed without affecting the CO_2 concentration. Porous Teflon filters that were provided with the NDIR analyzer are placed after sparging and before the analyzer to remove particulates while Nafion tubing (Perma Pure LLC MD-050 series dryer) is used for water vapor removal from the carrier stream.

Nafion contains a selectively permeable membrane that removes water vapor but retains CO_2. This membrane is made from a copolymer of tetrafluoroethylene (Teflon) and perfluoro-3 (6-dioxa-4-methyl-7-octene-sulfonic acid). These dryers are advertised as not requiring routine maintenance and having no moving parts. They are quick, continuous, and selective for the removal of water vapor from gas samples with high efficiency [69].

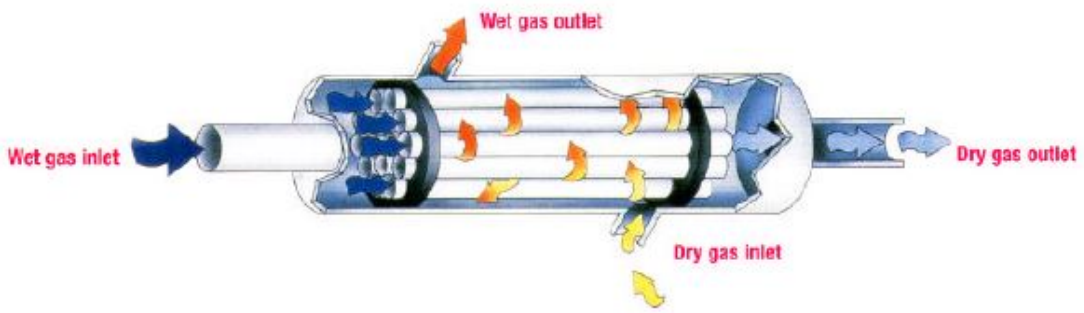

Figure 14: Nafion Dryer - The sample gas is dried as water vapor permeates through the interior walls of the Nafion tubing and is carried away by a drying gas.

The mechanism by which water vapor is removed is driven by the humidity difference between the walls of the Nafion tubing. Nafion is permeable to water vapor due to the presence of sulfonic acid. Each sulfonic acid group in the polymer can absorb up to 13 molecules of water. These acid groups absorb water vapor on the inside of the membrane

and carry them through ionic channels to the opposite surface where it is evaporated as shown in Figure 14. The moisture exchange occurs within a fraction of a second.

The interior layer of the Nafion dryer contains the sample gas. A drying gas flows continuously over the outside of this layer maintaining a pressure gradient and carrying away water vapor that has permeated through the interior wall. The drying gas is provided to the Nafion tubing from the same tank of compressed air as the sparging vessel and is controlled by a mechanical flow meter. The dried sample air then exits the water trap towards the NDIR analyzer.

2.6 LiCor 7000 CO_2/H_2O Analyzer

The Li-Cor 7000 is a versatile, high-accuracy [$\pm$ 1%], differential NDIR gas analyzer. It has a high signal-to-noise ratio (e.g., 25 ppb to 370 ppm for CO_2) and sensitivity allowing detection limits in the low-mid nM range. The analyzer can operate at the low flow rates demanded and can be applied for both laboratory and field testing.

The instrument contains a tungsten filament as its IR source. It uses a dichroic beam splitter as well as two solid state photonic IR light detectors to measure CO_2 and H_2O in the same gas stream. Bandpass optical filters are used to tune the sensor to the precise absorption bands of 4.255 μm for CO_2 and 2.595 μm for H_2O.

There are two cells that are used for gas analysis. The dried sample air containing the CO_2 is carried from the outlet of the Nafion water trap into Cell A of the Licor. Cell B of the Licor instrument is used as a zero reference. This cell contains a closed loop of air driven by the internal Licor pump. For a dry and carbonless reference, magnesium perchlorate and ascarite II filter out water vapor and carbon respectively. A thin layer of cotton separates the two substances while also functioning as a particulate remover. An additional teflon filter is placed in the reference cell loop to remove any lingering particulates.

The Licor is packaged with software for logging data to a Windows machine. A wide variety of parameters in addition to CO_2 and H_2O can be exported over USB or a serial connection. CO_2 concentrations can also be recorded in various units: parts per million (ppm or μmol per mol), partial pressure (Pa), a power signal (W), and absorptance (abs). Data is saved in a .txt file for processing.

The preferred unit for recording CO_2 from the LiCor is μmol per mol. This measurement can be converted into mol per L (M) to determine the amount of DOC in the liquid sample. The temperature and pressure readings from the LiCor as well as the ideal gas constant from Table 1 are used to calculate the volume for one mole of ideal gas (equation 10). The background signal at the LiCor is obtained by allowing a static sample at pH2 to degas. This near-zero value must be subtracted from the reported ppm value to remove noise (equation 11). The adjusted ppm value is then divided by the ideal gas volume calculated in (equation 10) to determine CO_2 in M (equation 11). If a DOC standard with a known value is used, the oxidation efficiency can be determined by comparing the expected CO_2 value to the reading from the NDIR analyzer (equation 12). The CO_2 oxidation efficiency values in Section 3.2 are determined with this method unless otherwise specified.

Quantity	Symbol	Unit
8.3145	R	J/mol
1	n	mole
Temperature	T	°K
Pressure	P	kPa

Table 1: Quantities for Ideal Gas Volume Calculation -
Temperature and pressure values for this calculation are provided the by LiCor non-dispersive infrared analyzer.

$$V\ [\frac{L}{mol}] = \frac{nRT}{P} \tag{10}$$

$$CO_2\ [Gas]\ [\frac{\mu mol}{L}] = \frac{CO_2\ [\frac{umol}{mol}] - CO_2\ Background\ [\frac{umol}{mol}]}{V} \tag{11}$$

$$Oxidation\ \% = \frac{CO_2\ [Gas]}{CO_2\ Standard\ Value\ [\frac{umol}{L}] \cdot \frac{Liquid\ \ flow\ \ rate\ [\frac{mL}{min}]}{Gas\ \ flow\ \ rate\ [\frac{mL}{min}]}} \tag{12}$$

2.7 Computer Controls

The motor driver and linear stage are connected to an Arduino micro-controller (Arduino Uno R3). The micro-controller processes the feedback from the linear stage and drives the motor through discrete step sequences. These steps can be programmed to output different liquid flow rates as required by the system. The Arduino processes user commands and delivers the desired step sequence to the motor. The code for the micro-controller can be seen in Appendix C. The wiring diagram for the micro-controller can be seen in Appendix D.

The Arduino code includes multiple functional modes for the syringe pump. The possible inputs are delivered to the Arduino through any computing device through a serial connection and include: pumping, refilling, braking, step sequence change, and flow rate change. The commands for each of these and their functions are listed in Table 2.

The Arduino also processes temperature readings from the thermocouple and manages the modified PI heat controller. The microcontroller provides a PWM signal to the mosfet to control the output to the heating wire at 12V. The set-point temperature for the heating system is slightly below boiling at 95°C.

The modified PI controller for the heating wire contains four heating modes. The first mode brings the temperature in the reaction chamber up quickly. During this mode the sensor reading is below 70°C and the PWM will be enabled at 100% duty cycle. The second

mode turns on a proportional controller from 70°C to 85°C. This controller slows down the heating process and brings the sensor value closer to the set-point. The third mode includes the PI controller for sensor values greater than 85°C. This PI controller brings the system to the set-point of 95°C. Finally, the PWM is forced to 0% duty cycle when the sensor value reaches 99°C to prevent possible boiling of the sample.

Input Command	Action
pump:X	Syringe pumps X amount in mL
refill:X	Syringe refills X amount in mL
empty	Syringe empties until front limit is reached
fill	Syringe fills up 150mL or until back limit is reached
rinse	Syringe fills and empties 3x
full	Motor put in full step mode
half	Motor put in half step mode
quarter	Motor put in quarter step mode
eighth	Motor put in eighth step mode
flow:X	Flow rate of syringe pump changed to X in mL per min
clear	Motor brakes

Table 2: Serial Interface Commands for Syringe Pump Control

A Raspberry Pi 3 (Model B) is used for logging from the Licor when a Windows PC is unavailable. It uses a python script to communicate with the Licor through its serial port. The python script saves the data to a .txt file which the Raspberry Pi can process through a spreadsheet program or other numerical computing environment.

The Raspberry Pi communicates with and programs the Arduino Uno via a USB interface. Commands and programming changes are delivered to the Arduino with the

Raspberry Pi. The Raspberry Pi fulfills the requirements of data logging and processing, programming, and user interaction for the system, thereby eliminating the need for a larger PC or laptop.

2.8 Chemical Samples and Reagents

The following chemical samples and reagents are used in the testing of this prototype. The acid for the degassing process is HCl (6N) made by Fisher Scientific (UN1789). As mentioned in Section 2.3 the chemical oxidant is a 30% w/w H_2O_2 and H_2O solution produced by Sigma Aldrich (H1009). DIC standards are made with H_2O and anhydronous sodium carbonate made by Nacalai Tesque (44936-42). DOC standards are made with H_2O and potassium hydrogen phthalate also made by Nacalai Tesque (44935-52). The pH indicator paper (pH 0.5 - 5.0) used was made by EMD Millpore (109560).

3 Results and Analysis

3.1 Stability

When oxidizing a given DOC sample, the stability of the CO_2 concentration in the gas stream delivered to the NDIR analyzer must be maintained for sub-μM analysis. This stability is mostly affected by flow rates both liquid and gas. These flow rates are influenced by mechanical interference, pressure and temperature changes.

The flow rate of the carrier gas is critical to signal stability at the CO_2 analyzer. Carrier gas flow rates to the sparging vessel are kept stable with the use of the MFC connected to a tank of compressed zero-grade air. The MFC displays its outputted flow rate in mL per min on the device. This flow rate does fluctuate slightly but the device meets the 1% accuracy listed in the specifications ($\pm$ 0.1 at 10 mL per min).

The syringe pump is designed to provide steady liquid flow rates $\leq$ 1 mL per min. The user sets the flow rate and can also increase the step sequence resolution of the motor. Each full step of the motor relates to 0.00025 inches of linear travel equaling 9.2 μL of liquid. With four steps in a fullstep sequence, each discrete step equates to 2.3 μL. Increasing the step resolution provides more steps per full step sequence thereby smoothing out the flow of liquid. Microstepping resolutions up to eighth stepping (32 steps per full step sequence or 0.2875 μL per step) are available to the motor through the Arduino code seen in Appendix C.

Extraction Efficiency

Tests were done to determine extraction efficiency based on sparging gas flow rates with a 2 mM DIC standard. The first design utilizing PDMS membrane inlet technology was not ideal in terms of extraction efficiency. Although these materials are useful for

removing dissolved gases from liquids, their extraction rates did not allow for the complete removal (100%) of CO_2 as desired for the system. The membranes also allowed large amounts water vapor to be separated from the liquid as the permeability coefficient for CO_2 (2.44 $[\frac{cm^3 \cdot cm}{cm^2 \cdot s \cdot Pa}]$) is approximately 9% to that of water vapor (27 $[\frac{cm^3 \cdot cm}{cm^2 \cdot s \cdot Pa}]$). The porous membrane inlet technology is not utilized due to these performance characteristics.

The second design utilizing the sparging vessel was used for all subsequent results. To test extraction efficiency as a function of gas flow rates, an arbitrary liquid flow rate of 1 mL per min was used and the expected CO_2 value (factoring in temperature, pressure, and H_2O signals at the NDIR sensor) is shown in Table 3. The Matlab code to determine these values is located in Appendix E. As expected, higher gas flow rates caused more efficient extraction. The liquid flow rate was reduced to achieve 100% extraction efficiency. An alternative method for potentially higher extraction efficiency is employing higher flow rates of gas with a different MFC.

Flow Rate (mL/min)	~Ramp Time (min)	Temp (°C)	Pressure (kPa)	H_2O (ppt)	CO_2 (ppm)	Expected CO_2 (ppm)	Extraction Efficiency (%)
1	90	25.44	101.36	3.96	18640	67300	27.7
2	52	25.43	101.29	2.24	17270	34900	49.5
3	26	24.67	102.22	1.78	14000	23300	60.1
4	21	24.42	102.50	0.57	11450	17500	65.3
5	12	24.88	102.18	0.85	10100	14100	71.5
10	9	25.05	102.49	0.33	5720	7100	80.5

Table 3: Extraction Efficiency in Sparging Vessel for a Liquid Flow Rate of 1 mL per min -
Reported factors: ramp time to plateau, temperature of the gas stream recorded by the LiCor non-dispersive infrared analyzer, gas pressure recorded by the LiCor, carbon dioxide concentration observed by the LiCor, expected concentration of carbon dioxide based upon dissolved inorganic concentration and flow rate of the aqueous sample, and extraction efficiency at varying extraction gas flow rates.

Residence Time

The residence time is a measurement of how long the sample must be sparged before all of the CO_2 is released from the sample. This parameter is dependent on the gas and liquid flow rates into the sparging vessel and is an important factor in determining the extraction efficiency of the system.

To determine the residence time, sample is pumped into the sparging vessel with a constant gas flow rate until a plateau signal is obtained at the analyzer. The pump is then stopped to allow the sample in the vessel to fully sparge. The residence time is determined from the the delay between when the pump is stopped to when CO_2 levels fall back to near-zero values. This value is dependent on the volume of sparging gas used and correlates with the flow rate of the gas.

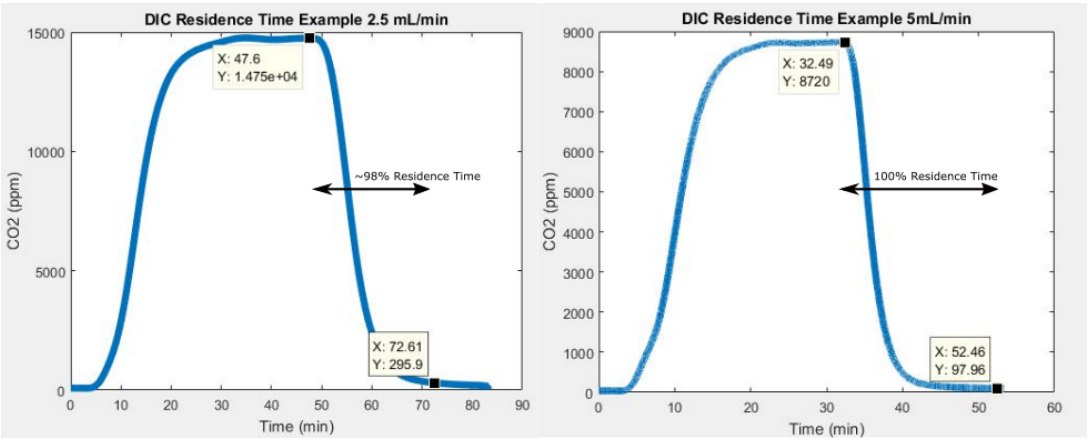

Figure 15: Residence Time Examples for 2 mmol Dissolved Inorganic Carbon Standard at Gas Flow Rates of 2.5 and 5 mL per min

Residence times tests were performed with a 2 mM DIC standard with gas flow rates of 2.5 and 5 mL per min displayed Figure 15. Approximately 100 mL of gas is necessary to fully sparge the sample volume of the sparging vessel although a considerable majority (98%) is removed after ∼60 mL as seen in the 2.5 mL per min example.

Signal Stability for DIC

To determine the analyzer signal stability during the sparging process, 2 mM DIC standards were placed through the sparging vessel. These standards were acidified to pH2 right before sparging. The following example in Figure 16 was sparged with a liquid flow rate of 1 mL per min and a gas flow rate of 5 mL per min. The signal had a plateau with a value of 414.7 $\pm$ 0.1 μM. Another example with the same liquid flow rate and a gas flow rate of 10 mL per min is also shown in Figure 15. This example had a signal at the plateau with a value of 233.5 $\pm$ 0.5 μM.

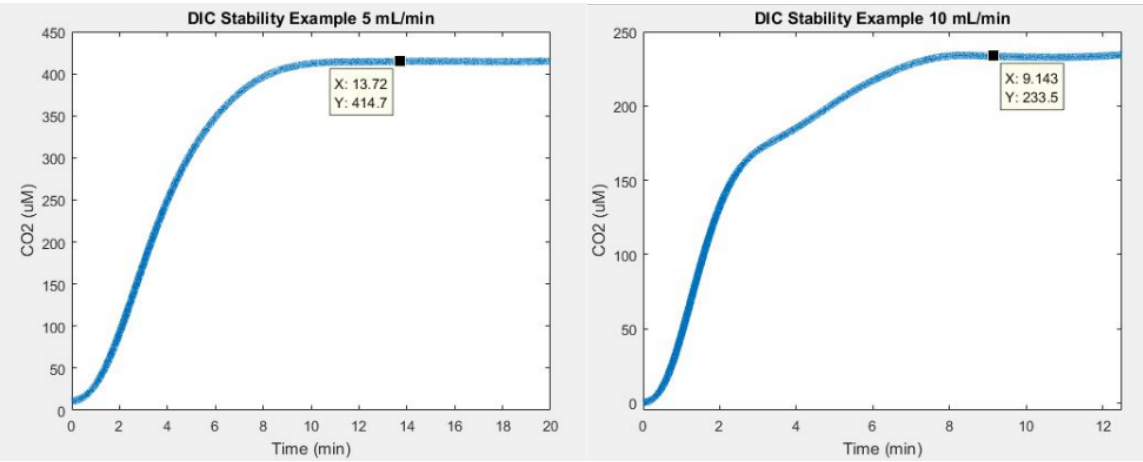

Figure 16: Stability Examples for 2 mmol Dissolved Inorganic Carbon Standard at Gas Flow Rates of 5 and 10 mL per min

These examples suggest that the sparging process is capable of delivering a stable signal with a small amount of drift as noted by the standard deviations.

Mechanical Interference, Temperature and Pressure Changes

Minimizing mechanical interference is crucial to the stability of DOC measurements. Mechanical interference in the system was primarily caused by the syringe pump. The

glass syringes that were used in the design showed significant leakage between the plunger and the inside of the syringe. The reported inner diameter of the syringe is 42.95 mm and the plunger diameter is listed at 42.8 mm. This 0.15 mm difference amounted to a leakage of around 0.085 grams per mL of 1000 μM DOC standard when the syringe was pumping at 1 mL per min. This leakage caused a significant amount of sample to be lost and presents a fault at the beginning of the system. It can also cause mechanical and pressure issues affecting the sample flow rate downstream. The leakage was not discovered until the syringe pump had been constructed and tested.

Increased temperatures in the oxidation chamber up to 100° C resulted in an increased oxidation efficiency. However temperatures greater than 100° C resulted in the sample boiling over and subsequent pressure and flow rate changes downstream in the system. For this reason the initial set-point temperature of 99° C was decreased to 95° C to prevent overshoot. Introducing active cooling is a possible solution to prevent any overshoot.

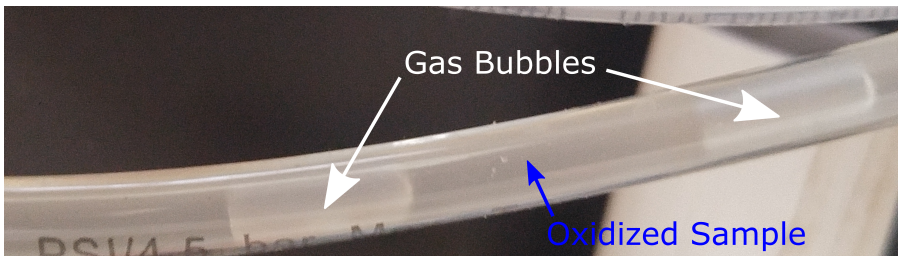

Figure 17: Gaseous Bubbles - The pockets of O_2 gas generated in the UV/H_2O_2 oxidation process affect signal stability.

UV interaction with H_2O_2 causes gaseous oxygen (equation 3) to separate from the liquid solution during oxidation. This creates bubbling effects in the reaction chamber associated with spontaneous changes in flow rates and causing pressure fluctuations downstream in the system. Pockets of gas accumulate in the quartz coil and can be seen exiting the reaction chamber going into the sparging vessel as shown in Figure 15. This gas also creates fluctuations in the sparging process, which further amplifies signal level fluctuations.

Signal Stability for DOC

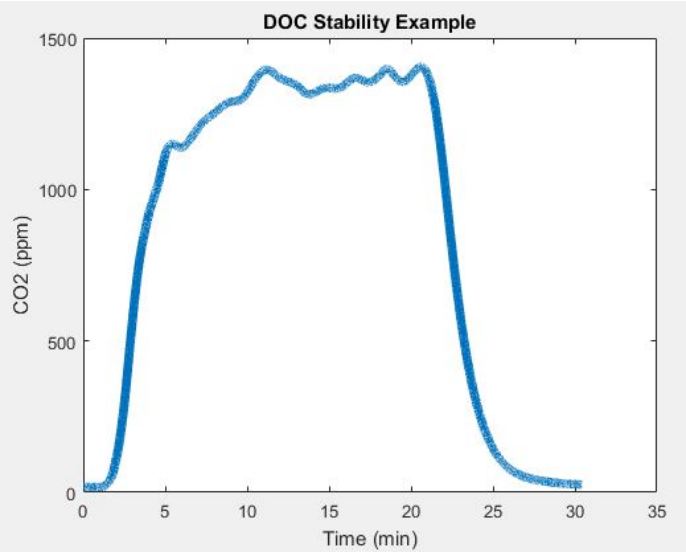

Figure 18: Dissolved Organic Carbon Stability Example with a 1000 μM Standard - Signal Fluctuation is Resultant from Effects of the Oxidation Process

DOC results showed difficulties in terms of signal stability. This is most likely due to the flow rate and pressure effects during the oxidation process as noted in Section 3.1.4. The following example shows an online test with a 1000 μM DOC standard shown in Figure 18. The signal stability at the plateau $\sim$1360 $\pm$ 24 μmol per mol. This signal fluctuation must be corrected for sub-μM DOC analysis.

3.2 Oxidation Efficiency

A primary goal in developing the system is the complete oxidation of DOC in marine samples. H_2O_2 concentrations, temperature, pH, and presence of halides, and irradiation time were all impacting factors on the oxidation efficiency. Their effects on the efficiency of the system were studied in order to produce higher levels of oxidation.

Oxidant Concentrations

Experiments were performed to determine the optimal H_2O_2 concentrations for both freshwater and high salinity samples. The samples used were 1000 μM DOC standards at pH2. These samples were run through the system with all other parameters the same including liquid (1 mL per min) and gas flow rates (10 mL per min). Oxidant concentrations in freshwater compared with oxidation efficiency can be seen in Figure 19 and Table 4.

NaCl was added to the DOC standard to reach a salinity of 35 grams per L. This high salinity value was chosen to simulate the salt contents of the ocean. The oxidation efficiency of oxidant concentrations at 35 grams per L can be seen in Table 5. The results show similar optimal H_2O_2 oxidant concentration both fresh and salt water in this system with a peak around 0.225%.

H_2O_2 Concentration (%)	CO_2 (ppm)	Oxidation Efficiency (%)
0.1	930.6 ± 3	37.2 ± 0.1
0.2	994.0 ± 15	40.0 ± 0.6
0.225	1052.5 ± 22	42.4 ± 0.6
0.25	1015.5 ± 13	40.7 ± 0.9
0.3	947.1 ± 23	37.9 ± 0.9
0.4	912.3 ± 18	36.3 ± 0.7
0.5	898.8 ± 32	36.0 ± 1.3
1.0	727.2 ± 6	28.9 ± 0.3
2.0	521.9 ± 13	20.6 ± 0.5

Table 4: Non-Dispersive Infrared Analyzer Values after Oxidation of 1000 μM Freshwater Dissolved Organic Carbon Standard with Varying Oxidant Concentrations

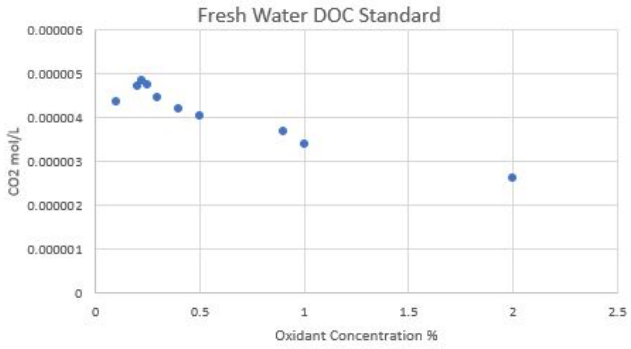

Figure 19: Optimal Hydrogen Peroxide Concentrations for 1000 μM Freshwater Dissolved Organic Carbon Standard

H_2O_2 Concentration (%)	CO_2 (ppm)	Oxidation Efficiency (%)
0.1	540.6 ± 9	19.5± 0.4
0.2	595.6 ± 14	23.6± 0.6
0.3	516.0 ± 8	20.4± 0.3
1.0	430.0 ± 7	16.8± 0.3
2.0	369.6 ± 6	14.4± 0.2

Table 5: Non-Dispersive Infrared Analyzer Values of High Salinity (35 grams per L) Samples after Oxidation with Varying Oxidant Concentrations

To determine if the quartz coil is adequate for UV irradiation of H_2O_2, the following calculations were performed. Using an optimal H_2O_2 concentration of 0.225% leads to 2.25 mL or 3.26 grams of H_2O_2 per L (equation 13). This equates to a molar concentration of 95.9 mM (equation 14). The reported molar extinction coefficient of H_2O_2 at 254 nm is 19.6 ± 0.3 (L per mol per cm) [45]. Using this molar extinction coefficient gives an absorbance of 1.88 ± 0.03 cm^{-1} (equation 15). According to the Beer-Lambert Law, an electromagnetic wave passing through a material loses intensity as a function of depth (equation 16). The penetration depth at which the intensity of the 254 nm UV light reaches half its initial value would be 0.369 cm (equation 17). With the quartz coil in the system having UV

transparency at 254 nm and an inner diameter of 1 mm, this depth requirement should be satisfied.

$$\begin{aligned} Density\ of\ H_2O_2: \quad & \rho = 1.45\ [\frac{g}{mL}] \\ H_2O_2\ per\ L: \quad & 0.00225 \cdot 1000\ [\frac{mL}{L}] = 2.25\ [\frac{mL}{L}] \\ & 2.25\ [\frac{mL}{L}] \cdot \rho = 3.26\ [\frac{g}{L}] \end{aligned} \tag{13}$$

$$\begin{aligned} H_2O_2\ Molar\ Weight: \quad & 34.0147\ [\frac{g}{mol}] \\ H_2O_2\ Mole\ per\ L: \quad & \frac{3.26\ [\frac{g}{L}]}{34.0\ [\frac{g}{mol}]} = 0.0959\ [\frac{mol}{L}] \end{aligned} \tag{14}$$

$$\begin{aligned} H_2O_2\ Molar\ Extinction\ at\ 254\ nm: \quad & \epsilon = 19.6 \pm 0.3\ [\frac{L}{mol \cdot cm}] \\ H_2O_2\ Absorbance\ at\ 254\ nm: \quad & \epsilon \cdot 0.0959\ [\frac{mol}{L}] = 1.880 \pm 0.03\ [cm^{-1}] \end{aligned} \tag{15}$$

$$I = I_0 \cdot e^{-\epsilon \cdot concentration \cdot length} \tag{16}$$

$$\begin{aligned} 0.5 &= e^{-\epsilon \cdot concentration \cdot length} \\ ln(0.5) &= -\epsilon \cdot concentration \cdot length \\ length &= \frac{ln(0.5)}{-1.880\ [cm^{-1}]} = 0.369\ [cm] \end{aligned} \tag{17}$$

Temperature

The oxidation efficiency of the system was compared with and without the feedback-controlled heating system connected. Due to the heat generating capabilities of the UV lamp in the insulated reaction chamber, the set point temperature of 95° C was approximately reached in both cases. However the temperature decreased when the heating system was disconnected due to the sample injected into the reaction chamber. In the case of a

liquid flow rate of 1.0 mL per min, the equilibrium temperature of the reaction chamber with the heating system disconnected dropped to approximately ∼85°C.

A 1000 μM DOC standard was run through the system at pH2 with a liquid flow rate of 1.0 mL per min and gas flow rate of 10.0 mL per min to determine temperature effects n oxidation efficiency. Triplicates of the standard were run through the system and shown in Table 6. The results show a slight increase in the oxidation efficiency due to the ∼10°C temperature difference.

Test	Heater Off (85°C) (ppm)	Oxidation (%)	Heater On (95°C) (ppm)	Oxidation (%)
1	1265 ± 16	51.0 ± 0.7	1360 ± 24	55.2 ± 1.0
2	1217 ± 29	53.5 ± 1.2	1355 ± 31	55.0 ± 1.3
3	1330 ± 19	54.0 ± 0.8	1305 ± 30	52.6 ± 1.3
Average	1304 ± 21	52.8 ± 0.9	1340 ± 28	54.3 ± 1.1

Table 6: Oxidation Efficiency of 1000 μM Dissolved Organic Carbon Standard with Temperature Control Off vs On

Freshwater Oxidation Efficiency

Experiments show that approximately 100% DOC oxidation for freshwater samples was achieved. This oxidation efficiency was achieved by taking into account the residence time requirement, using an optimal oxidant concentration, and enabling temperature control.

This can be seen in the following example: a 100 μM DOC standard was run through the system with a liquid flow rate of 0.5 mL per min and sparged with a gas flow rate of 10 mL per min to obtain 100% extraction. The 100 μM standard was obtained from diluting a 1000 μM standard when there was a small amount of the 1000 μM standard remaining.

The signal obtained at the LiCor had an average ppm value of 134.3 ± 3.7 with a temperature of 25.27 ± 0.06°C and pressure of 101.857 ± 0.004 kPa. The baseline value

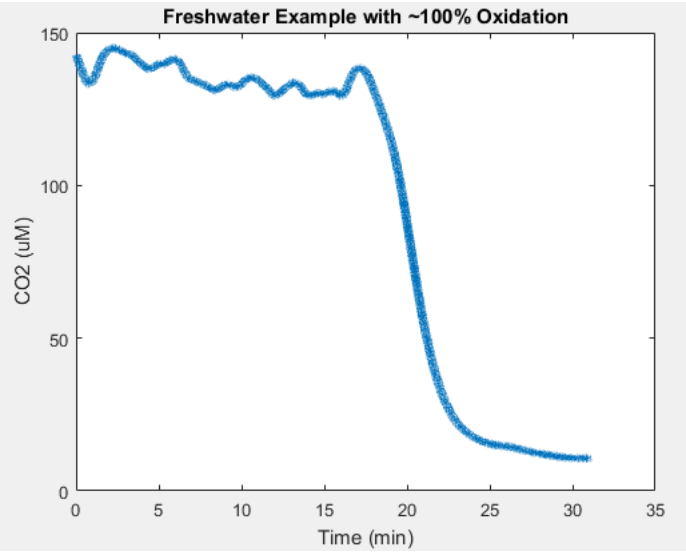

Figure 20: Example of 100% Dissolved Organic Carbon Oxidation with Freshwater

for this sample was 10.5 ppm. Using (equations 10 - 12) this leads to a calculated oxidation efficiency of 101.7 ± 3.1 %. The error in the calculated oxidation efficiency and the large standard deviation are due to signal fluctuation shown in Figure 20.

Halide Interference

Salinity had a strong negative effect by reducing the oxidation efficiency. Oxidation was performed with varying salinity levels on a 1000 μM DOC standard to determine its effect. Each test was performed at pH2 with the same liquid and gas flow rates (1 and 10 mL per min respectively). The results of these tests along with their loss in oxidation efficiency compared to the freshwater sample are shown in the following Table 7 and Figure 21. Tests showed that higher salinity samples related to reduced oxidation efficiency but the effect was not linear.

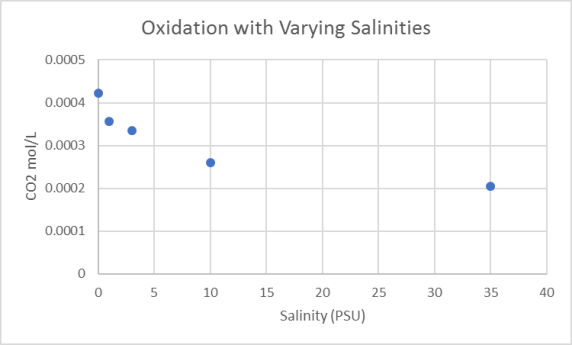

Figure 21: Dissolved Organic Carbon Oxidation Efficiency of 1000 μM Standards with Varying Salinities

Salinity (grams per L)	CO_2 (ppm)	Efficiency Loss (%)
0	905.9 $\pm$ 19	NA
1	781.7 $\pm$ 11	13.7
3	720.5 $\pm$ 16	20.5
10	552.5 $\pm$ 14	39.0
35	441.3 $\pm$ 11	51.3

Table 7: Oxidation Efficiency vs Salinity

pH Effects

Studies have shown that pH affects the extent and rate of photo oxidation on organic compounds [70]. Below an initial pH of 5, photo oxidation rates are pH sensitive and slowed considerably [16].

Experiments were performed to better understand the effects of pH on oxidation efficiency in the system. Saline samples were taken from the dock at the Skidaway Institute of Oceanography. These samples (with salinities of 25 grams per L and DOC concentration of 303.6 μM) were run through the oxidation system at pH2 and at natural pH8 with all other parameters the same (i.e., oxidant concentration, temperature, liquid flow rates).

After oxidation the natural pH samples were acidified to pH2 to release the oxidized DOC from the solution as CO_2 prior to analysis. The amount of DOC remaining in the samples was measured to determine the oxidation efficiency at these pH. Results were run through a commercial instrument (Shimadzu TOC-V_{CPH}) and can be seen in the following Table 8. Freshwater 100 μM standards were also tested.

Methods were not introduced to enable the online measurement of high pH samples through this system. If high pH samples are acidified and sparged after oxidation, the system is unable to distinguish between DIC and the oxidized DOC. If samples are acidified and purged of DIC prior to oxidation, they must be alkalified back to high pH before oxidation without introducing contaminants.

To determine finer pH effects on oxidation efficiency, a different batch of dock samples was acidified with different amounts of HCl and pH indicator paper (0.5 - 5.0) was used to determine their approximate pH. These samples had a base DOC concentration of 159.0 μM and were run through the oxidation chamber with all parameters the same except for pH. After oxidation, the samples were brought to pH$\leq$2 and analyzed using the Shimadzu TOC-V_{CPH} shown in Table 9.

Sample	DOC Concentration (μM)
Fresh No Oxidation	103.44
Fresh pH2	89.25
Fresh pH7	42.53
Saline No Oxidation	303.59
Saline pH2	266.34
Saline Natural pH	247.52

Table 8: Dissolved Organic Carbon Remaining after Oxidation of 100 μM Freshwater Standards and Dock Samples at Natural pH vs pH2

Sample	DOC Concentration (μM)
No Oxidation	159.0
∼pH1.8	153.9
pH2	146.0
pH3	129.0
pH4	123.7
pH5	118.4
∼pH5.5	109.6

Table 9: Dissolved Organic Carbon Remaining after Oxidation of Dock Samples at Varying pH Values

UV Irradiation Time

A batch of saline samples (with a salinity of $\sim$ 25 grams per L) was taken from the dock at the Skidaway Institute of Oceanography were pumped through the system at varying liquid flow rates to compare oxidation efficiency with respect to irradiation time. These samples were run through the system with all other factors (i.e., oxidant concentration, pH, salinity, gas flow rates, and temperature) the same.

The samples were all run through the oxidation chamber at their natural pH (∼pH8). The samples were acidified after oxidation causing DIC and the oxidized CO_2 to be released. The remaining DOC concentrations can be seen in Figure 22 and Table 10. These results were determined using the Shimadzu TOC-V_{CPH} due to the inability of the system to isolate DOC after oxidation at high pH.

There was a good correlation between irradiation time and the DOC oxidized. Longer irradiation times predictably led to higher oxidation efficiency but with diminishing returns. There was a power law relationship between irradiation time and oxidation efficiency shown in Figure 22 with an R^2 of 0.96.

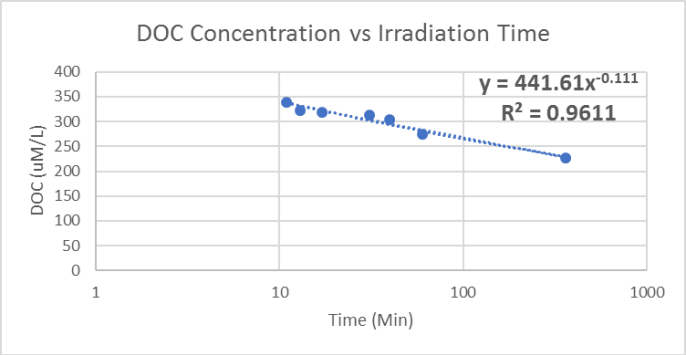

Figure 22: Dissolved Organic Carbon Remaining after Oxidation of Dock Samples at Varying Irradiation Times

Irradiation Time (min)	DOC Concentration Remaining (μM)
11	339.24
13	322.97
17	317.75
31	313.17
40	304.36
60	275.05
360	227.41

Table 10: Oxidation Efficiency vs Irradiation Time

4 Discussion

This UV-WCO system achieved approximately 100% DOC oxidation for freshwater samples but must be improved for precision analysis and to achieve 100% DOC oxidation for saline samples. The following suggestions for improving signal stability and oxidation efficiency should be explored and optimized to meet these goals.

4.1 Improving Signal Stability

The Cadence G5331 dissolved gas analysis syringe was not gas-tight and this mechanical flaw causes sample loss and possible signal fluctuation at the NDIR analyzer. A glass syringe without leakage should be employed in the system for more stability. The controls and mechanical construction of the syringe pump can be adapted to fit a fluid-tight syringe.

The bubbling effect generated by the H_2O_2 interaction with UV photo oxidation must be limited to stabilize the signal at the NDIR analyzer. This is difficult due to the oxidated CO_2 present in these bubbles that must be preserved for analysis. A different chemical oxidant could eliminate the bubbling effect in the oxidized sample.

4.2 Improving Oxidation Efficiency

Further experiments must be conducted in order to achieve the goal of 100% oxidation efficiency in marine samples. Extending the irradiation time, using a stronger lamp, finer pH controls, catalytic oxidation, and different chemical oxidants (e.g., ammonium persulfate) are possible methods to achieve higher efficiency.

Optimizing Irradiation Time

Lowering liquid flow rates leads to longer irradiation times and stronger oxidation efficiency. However this is not feasible at long periods due to diminishing returns. Using the

equation provided by the irradiation time test, it would take approximately 10^{21} hours to reach 100% oxidation for that batch of dock samples. Irradiation times can be reduced with the use of a stronger lamp due to the UV dependence of the oxidation system.

Optimizing Photo Oxidation

Higher powered lamps increase the photons per unit time radiating on the sample leading to a higher oxidation efficiency given the same irradiation time and spectral output. A lamp with the largest UV output at 254 and 185 nm is recommended to help reduce irradiation times. The 10W lamp (GPH212T5VH) in this system outputs 2.7 W at 254 nm. The same manufacturer makes a 79W lamp with the same spectral output (GPH1630T5V) which provides 34.5W at 254 nm. This higher-powered lamp would provide more photons per unit time but has disadvantages in terms of size (1.63 m) and voltage requirement (189 V). The reaction chamber can be redesigned to meet the demands of a larger and more powerful lamp.

Along with a more powerful lamp, liquid flow rates should be optimized to a minimum value allowing for longer irradiation times while still providing steady liquid flow rates for sparging and signal stability.

Optimizing with pH Control

The pH effects on oxidation efficiency are more difficult to optimize due to the possibility of contamination from inorganic sources. Samples must be decarbonated of DIC prior to analysis and it is possible to do this up to pH values of 5 [16].

One method involves acidifying samples under pH5 and removing DIC before raising the pH using a carbon-free buffer. The sample would be oxidized at this raised pH but then require re-acidification to sparge the oxidized DOC from the liquid. Applying a proper

buffer would be difficult as strong alkali buffers can not be used due to the large amounts of carbon contamination they could introduce. Sodium tetraborate is suggested as a possible buffer. The fine pH control required in this process would potentially be challenging and time consuming.

Catalytic Oxidation

A catalyst could further enhance the oxidation efficiency in the system. Mercury (Hg^{+2}), Aluminum - Iron (Al-Fe) pillared clay, and beidellite are possible catalysts for enhancing WCO efficiency in the system. Hg^{+2} can effect oxidation kinetics by forming stable complexes with halide ions and countering their inhibitory effect [71]. Al-Fe is shown to be an efficient solid catalyst to oxidize organic compounds in water by hydrogen peroxide without significant catalyst leaching [72]. Beidellite has also been observed as an effective catalyst for the wet H_2O_2 oxidation of phenolic aqueous wastes [73]. The inclusion of any of these catalysts is primarily dependent on their ability not to add carbon contamination to the sample. Increased oxidation efficiency and ease of inclusion to the system would be examined if carbon contamination is non-existent.

Possible Alternative Chemical Oxidants

There exist many possible chemical oxidants that can be used for this UV-WCO system. H_2O_2 was chosen for its relative safety, cost, and oxidative properties. However it may not be the most optimal chemical oxidant to achieve 100% oxidation for high salinity samples. Ammonium persulfate has been a preferred chemical oxidant for WCO DOC analyzers [74]. Persulfate oxidation is dependent on the formation of sulfate radicals by photolysis or thermolysis but these radicals also suffer competition by halides such as chlorine [75]. Although ammonium persulfate is effective at DOC oxidation, it has disadvantages as it is

highly flammable, explosive, and toxic when inhaled [76]. It must be optimized in a similar fashion as H_2O_2 due to the effect of chlorine interference.

5 Conclusions

This thesis presents attempts at optimizing a prototype DOC analyzer for high salinity samples. Although 100% DOC oxidation for freshwater samples was achieved, there were difficulties in signal stability and oxidation efficiency for saline samples. The UV-WCO system described can be adapted to overcome some of these difficulties and ideally provide precise sub-μM analysis. Analysis at this precision would meet the demands of the marine science community for the quantification of small changes in DOC.

The suggestions made in the discussion section should be explored and optimized. A combination of some or all of these alternatives could help reach the goal of 100% DOC oxidation for marine samples with a stable and precise (sub-μM) signal:

- a fluid tight syringe
- a more powerful UV lamp
- pH control without carbon contamination
- catalytic oxidation without carbon contamination
- a different chemical oxidant

References

[1] K. Mopper, "Photochemical source of biological substrates in sea water: implications for carbon cycling," *Nature*, vol. 341, pp. 637–639, 1989.

[2] H. Craig, "Son of abyssal carbon," *Journal of Geophysical Research*, vol. 76, no. 21, pp. 5133–5139, 1971.

[3] J. H. Sharp, C. A. Carlson, E. T. Peltzer, D. M. Castle-Ward, K. B. Savidge, and K. R. Rinker, "Final dissolved organic carbon broad community intercalibration and preliminary use of DOC reference materials," *Marine Chemistry*, vol. 77, no. 4, pp. 239–253, 2002.

[4] J. H. Sharp, R. Benner, L. Bennett, C. A. Carlson, S. E. Fitzwater, E. T. Peltzer, and L. M. Tupas, "Analyses of dissolved organic carbon in seawater: the JGOFS EqPac methods comparison," *Marine Chemistry*, vol. 48, no. 2, pp. 91–108, 1995.

[5] F. Wu, D. Kothawala, R. Evans, P. Dillon, and Y. Cai, "Relationships between doc concentration, molecular size and fluorescence properties of dom in a stream," *Applied Geochemistry*, vol. 22, no. 8, pp. 1659–1667, 2007.

[6] J. I. Hedges, "Global biogeochemical cycles: progress and problems," *Marine chemistry*, vol. 39, no. 1-3, pp. 67–93, 1992.

[7] J. I. Hedges, "Why dissolved organics matter," *Biogeochemistry of marine dissolved organic matter*, pp. 1–33, 2002.

[8] IPCC, "Ipcc, 2001: Climate change 2001: impacts, adaptation and vulnerability," *International Journal of Climatology*, vol. 22, no. 10, pp. 1285–1286, 2002.

[9] D. Hansell, "Dissolved organic carbon export with North Pacific Intermediate Water formation," *Global Biogeochemical Cycles*, vol. 16, pp. 7–1–7–8, Feb. 2002.

[10] J. Arstegui, C. M. Duarte, S. Agust, M. Doval, X. A. lvarez Salgado, and D. A. Hansell, "Dissolved organic carbon support of respiration in the dark ocean," *Science*, vol. 298, no. 5600, pp. 1967–1967, 2002.

[11] P. J. Wangersky, "Measurement of organic carbon in seawater," *ACS Publications*, 1975.

[12] R. M. Gershey, M. D. Mackinnon, P. l. B. Williams, and R. M. Moore, "Comparison of three oxidation methods used for the analysis of the dissolved organic carbon in seawater," *Marine Chemistry*, vol. 7, no. 4, pp. 289–306, 1979.

[13] Y. Sugimura and Y. Suzuki, "A high-temperature catalytic oxidation method for the determination of non-volatile dissolved organic carbon in seawater by direct injection of a liquid sample," *Marine Chemistry*, vol. 24, no. 2, pp. 105–131, 1988.

[14] I. R. Wilson and G. M. Harris, "The oxidation of thiocyanate ion by hydrogen peroxide. II. The acid-catalyzed reaction," *Journal of the American Chemical Society*, vol. 83, no. 2, pp. 286–289, 1961.

[15] D. W. Menzel and R. F. Vaccaro, "The measurement of dissolved organic and particulate carbon in seawater," *Limnology and Oceanography*, vol. 9, no. 1, pp. 138–142, 1964.

[16] K. Collins, P. Le, and B. Williams, "An automated photochemical method for the determination of dissolved organic carbon in sea and estuarine waters," *Marine chemistry*, vol. 5, no. 2, pp. 123–141, 1977.

[17] C. L. Osburn and G. StJean, "The use of wet chemical oxidation with highamplification isotope ratio mass spectrometry (WCOIRMS) to measure stable isotope values of dissolved organic carbon in seawater," *Limnology and Oceanography: Methods*, vol. 5, no. 10, pp. 296–308, 2007.

[18] J. H. McKenna and P. H. Doering, "Measurement of dissolved organic carbon by wet chemical oxidation with persulfate: influence of chloride concentration and reagent volume," *Marine Chemistry*, vol. 48, no. 2, pp. 109–114, 1995.

[19] J. L. Weishaar, G. R. Aiken, B. A. Bergamaschi, M. S. Fram, R. Fujii, and K. Mopper, "Evaluation of specific ultraviolet absorbance as an indicator of the chemical composition and reactivity of dissolved organic carbon," *Environmental science & technology*, vol. 37, no. 20, pp. 4702–4708, 2003.

[20] G. Spyres, M. Nimmo, P. J. Worsfold, E. P. Achterberg, and A. E. Miller, "Determination of dissolved organic carbon in seawater using high temperature catalytic oxidation techniques," *TrAC Trends in Analytical Chemistry*, vol. 19, no. 8, pp. 498–506, 2000.

[21] C. A. Carlson, S. J. Giovannoni, D. A. Hansell, S. J. Goldberg, R. Parsons, and K. Vergin, "Interactions among dissolved organic carbon, microbial processes, and community structure in the mesopelagic zone of the northwestern sargasso sea," *Limnology and Oceanography*, vol. 49, no. 4, pp. 1073–1083, 2004.

[22] K. Mopper, X. Zhou, R. J. Kieber, D. J. Kieber, R. J. Sikorski, and R. D. Jones, "Photochemical degradation of dissolved organic carbon and its impact on the oceanic carbon cycle," *Nature*, vol. 353, no. 6339, pp. 60–62, 1991.

[23] T. Reinthaler, X. A. lvarez Salgado, M. lvarez, H. M. van Aken, and G. J. Herndl, "Impact of water mass mixing on the biogeochemistry and microbiology of the Northeast Atlantic Deep Water," *Global Biogeochemical Cycles*, vol. 27, no. 4, pp. 1151–1162, 2013.

[24] R. Benner and M. Strom, "A critical evaluation of the analytical blank associated with DOC measurements by high-temperature catalytic oxidation," *Marine Chemistry*, vol. 41, no. 1-3, pp. 153–160, 1993.

[25] A. Miller, *A reassessment of the determination of dissolved organic carbon in natural waters using high temperature catalytic oxidation.* PhD thesis, Ph. D. thesis, The University of Liverpool, 1996.

[26] A. McNichol, E. Osborne, A. Gagnon, B. Fry, and G. Jones, "TIC, TOC, DIC, DOC, PIC, POC unique aspects in the preparation of oceanographic samples for 14c-AMS," *Nuclear Instruments and Methods in Physics Research Section B: Beam Interactions with Materials and Atoms*, vol. 92, pp. 162–165, June 1994.

[27] E. Mearns, "The carbon cycle: a geologists view," 2014.

[28] P. J. Wangersky, "Dissolved organic carbon methods: a critical review," *Marine Chemistry*, vol. 41, no. 1, pp. 61–74, 1993.

[29] B. Fry, E. Peltzer, C. Hopkinson, A. Nolin, and L. Redmond, "Analysis of marine doc using a dry combustion method," *Marine Chemistry*, vol. 54, no. 3-4, pp. 191–201, 1996.

[30] C. Wiebinga and H. De Baar, "Determination of the distribution of dissolved organic carbon in the indian sector of the southern ocean," *Marine Chemistry*, vol. 61, no. 3, pp. 185–201, 1998.

[31] D. A. Hansell, "Dissolved Organic Carbon Reference Material Program," *Eos, Transactions American Geophysical Union*, vol. 86, pp. 318–318, Aug. 2005.

[32] J. C. Crittenden, S. Hu, D. W. Hand, and S. A. Green, "A kinetic model for H2o2/UV process in a completely mixed batch reactor," *Water Research*, vol. 33, pp. 2315–2328, July 1999.

[33] H. Mueller and W. M. Bandaranayake, "An automated method for the determination of dissolved organic carbon in seawater using continuous thin-film UV oxidation," *Marine Chemistry*, vol. 12, no. 1, pp. 59–68, 1983.

[34] F. A. J. Armstrong, P. M. Williams, and J. H. Strickland, "Photo-oxidation of organic matter in sea water by ultra-violet radiation, analytical and other applications," *Nature*, vol. 211, no. 5048, pp. 481–483, 1966.

[35] C. M. Sharpless and K. G. Linden, "Experimental and model comparisons of low-and medium-pressure Hg lamps for the direct and H2o2 assisted UV photodegradation of N-nitrosodimethylamine in simulated drinking water," *Environmental Science & Technology*, vol. 37, no. 9, pp. 1933–1940, 2003.

[36] T. Bintsis, E. Litopoulou-Tzanetaki, and R. K. Robinson, "Existing and potential applications of ultraviolet light in the food industry–a critical review," *Journal of the Science of Food and Agriculture*, vol. 80, no. 6, pp. 637–645, 2000.

[37] W. Han, W. Zhu, P. Zhang, Y. Zhang, and L. Li, "Photocatalytic degradation of phenols in aqueous solution under irradiation of 254 and 185nm uv light," *Catalysis Today*, vol. 90, no. 3, pp. 319–324, 2004.

[38] S. A. Huber and F. H. Frimmel, "Flow injection analysis for organic and inorganic carbon in the low-ppb range," *Analytical Chemistry*, vol. 63, no. 19, pp. 2122–2130, 1991.

[39] M. Kavanaugh, Z. K. Chowdhury, S. Kommineni, S. Liang, J. Min, J.-P. Croue, N. Corin, G. Amy, E. Simon, and W. Cooper, *Removal of MTBE with advanced oxidation processes*. Iwa publishing, 2004.

[40] S. R. Cater, M. I. Stefan, J. R. Bolton, and A. Safarzadeh-Amiri, "UV/H2o2 treatment of methyl tert-butyl ether in contaminated waters," *Environmental science & technology*, vol. 34, no. 4, pp. 659–662, 2000.

[41] J. C. Kruithof, P. C. Kamp, and M. Belosevic, "UV/H2o2-treatment: the ultimate solution for pesticide control and disinfection," *Water science and technology: water supply*, vol. 2, no. 1, pp. 113–122, 2002.

[42] E. J. Rosenfeldt, B. Melcher, and K. G. Linden, "UV and UV/H2o2 treatment of methylisoborneol (MIB) and geosmin in water," *Journal of Water Supply: Research and Technology-AQUA*, vol. 54, no. 7, pp. 423–434, 2005.

[43] G. Cauwet, "Automatic determination of dissolved organic carbon in seawater in the sub-ppm range," *Marine Chemistry*, vol. 14, no. 4, pp. 297–306, 1984.

[44] Y.-S. Shen, Y. Ku, and K.-C. Lee, "The effect of light absorbance on the decomposition of chlorophenols by ultraviolet radiation and UV/H2o2 processes," *Water research*, vol. 29, no. 3, pp. 907–914, 1995.

[45] USPTechnologies, "Ultraviolet absorption spectrum, hydrogen peroxide," 2017.

[46] O. C. Zafiriou, J. Joussot-Dubien, R. G. Zepp, and R. G. Zika, "Photochemistry of natural waters," *Environmental Science & Technology*, vol. 18, no. 12, pp. 358A–371A, 1984.

[47] P. L. Brezonik and J. Fulkerson-Brekken, "Nitrate-induced photolysis in natural waters: controls on concentrations of hydroxyl radical photo-intermediates by natural scavenging agents," *Environmental Science & Technology*, vol. 32, no. 19, pp. 3004–3010, 1998.

[48] G. V. Buxton, C. L. Greenstock, W. P. Helman, and A. B. Ross, "Critical review of rate constants for reactions of hydrated electrons, hydrogen atoms and hydroxyl radicals OH/O in aqueous solution," *Journal of physical and chemical reference data*, vol. 17, no. 2, pp. 513–886, 1988.

[49] A. S. Stasinakis, "Use of selected advanced oxidation processes (AOPs) for wastewater treatmenta mini review," *Global NEST Journal*, vol. 10, no. 3, pp. 376–385, 2008.

[50] S. R. Beaupre, E. R. M. Druffel, and S. Griffin, "A low-blank photochemical extraction system for concentration and isotopic analyses of marine dissolved organic carbon," *Limnology and Oceanography: Methods*, vol. 5, no. 6, pp. 174–184, 2007.

[51] L. Li, Z. Xiao, S. Tan, L. Pu, and Z. Zhang, "Composite pdms membrane with high flux for the separation of organics from water by pervaporation," *Journal of Membrane Science*, vol. 243, no. 1, pp. 177–187, 2004.

[52] S. Kaltin, "A rapid method for determination of total dissolved inorganic carbon in seawater with high accuracy and precision," *Marine Chemistry*, vol. 96, pp. 53–60, Nov. 2005.

[53] R. S. Matthews and F. E. Witherell Jr, "Carbon dioxide sensor," July 25 1989. US Patent 4,851,195.

[54] S. Neethirajan, D. Jayas, and S. Sadistap, "Carbon dioxide (co2) sensors for the agrifood industrya review," *Food and Bioprocess Technology*, vol. 2, no. 2, pp. 115–121, 2009.

[55] M. J. Tierney and H. O. L. Kim, "Electrochemical gas sensor with extremely fast response times," *Analytical Chemistry*, vol. 65, no. 23, pp. 3435–3440, 1993.

[56] W. J. Aston and Y. S. Chan, "Electrochemical gas sensor," Mar. 7 1995. US Patent 5,395,507.

[57] R. Zhou, S. Vaihinger, K. Geckeler, and W. Göpel, "Reliable co2 sensors with silicon-based polymers on quartz microbalance transducers," *Sensors and Actuators B: Chemical*, vol. 19, no. 1-3, pp. 415–420, 1994.

[58] H. Kimoto, K. NozAKI, S. KUDo, K. KATO, A. NEGISHI, and H. KAYANNE, "Achieving high time-resolution with a new flow-through type analyzer for total inorganic carbon in seawater," *Analytical sciences*, vol. 18, no. 3, pp. 247–253, 2002.

[59] T. J. Cunningham, "Infrared detector system with controlled thermal conductance," Oct. 17 2000. US Patent 6,133,572.

[60] R. Rubio, J. Santander, L. Fonseca, N. Sabate, I. Gracia, C. Cane, S. Udina, and S. Marco, "Non-selective ndir array for gas detection," *Sensors and Actuators B: Chemical*, vol. 127, no. 1, pp. 69–73, 2007.

[61] R. Whatmore, A. Patel, N. Shorrocks, and F. Ainger, "Ferroelectric materials for thermal ir sensors state-of-the-art and perspectives," *Ferroelectrics*, vol. 104, no. 1, pp. 269–283, 1990.

[62] J. Herrn, G. G. Mandayo, and E. Castao, "Solid state gas sensor for fast carbon dioxide detection," *Sensors and Actuators B: Chemical*, vol. 129, no. 2, pp. 705 – 709, 2008.

[63] H. Nara, H. Tanimoto, Y. Tohjima, H. Mukai, Y. Nojiri, K. Katsumata, and C. Rella, "Effect of air composition (n2, o2, ar, and h2o) on co2 and ch4 measurement by wavelength-scanned cavity ring-down spectroscopy: calibration and measurement strategy," *Atmospheric Measurement Techniques*, vol. 5, no. 11, p. 2689, 2012.

[64] G. Zhang and X. Wu, "A novel co 2 gas analyzer based on ir absorption," *Optics and Lasers in Engineering*, vol. 42, no. 2, pp. 219–231, 2004.

[65] G. Korotcenkov, "Handbook of gas sensor materials," *Properties, Advantages and*, 2013.

[66] J. Y. Wong and M. Schell, "Zero drift ndir gas sensors," *Sensor Review*, vol. 31, no. 1, pp. 70–77, 2011.

[67] A. Körtzinger, L. Mintrop, D. W. Wallace, K. M. Johnson, C. Neill, B. Tilbrook, P. Towler, H. Y. Inoue, M. Ishii, G. Shaffer, *et al.*, "The international at-sea intercomparison of fco 2 systems during the r/v meteor cruise 36/1 in the north atlantic ocean," *Marine Chemistry*, vol. 72, no. 2, pp. 171–192, 2000.

[68] K. Kutschera, H. Börnick, and E. Worch, "Photoinitiated oxidation of geosmin and 2-methylisoborneol by irradiation with 254nm and 185nm uv light," *Water Research*, vol. 43, no. 8, pp. 2224–2232, 2009.

[69] N. G. Sundin, J. F. Tyson, C. P. Hanna, and S. A. McIntosh, "The use of nafion dryer tubes for moisture removal in flow injection chemical vapor generation atomic absorption spectrometry," *Spectrochimica Acta Part B: Atomic Spectroscopy*, vol. 50, no. 4-7, pp. 369–375, 1995.

[70] B. Manny, M. Miller, and R. Wetzel, "Ultraviolet combustion of dissolved organic nitrogen compounds in lake waters," *Limnology and Oceanography*, vol. 16, no. 1, pp. 71–85, 1971.

[71] J. E. Bauer, M. L. Occelli, P. M. Williams, and P. C. McCaslin, "Heterogeneous catalyst structure and function: review and implications for the analysis of dissolved organic carbon and nitrogen in natural waters," *Marine chemistry*, vol. 41, no. 1, pp. 75–89, 1993.

[72] J. Barrault, M. Abdellaoui, C. Bouchoule, A. Majesté, J. Tatibouët, A. Louloudi, N. Papayannakos, and N. Gangas, "Catalytic wet peroxide oxidation over mixed (al–fe) pillared clays," *Applied Catalysis B: Environmental*, vol. 27, no. 4, pp. L225–L230, 2000.

[73] C. Catrinescu, C. Teodosiu, M. Macoveanu, J. Miehe-Brendlé, and R. Le Dred, "Catalytic wet peroxide oxidation of phenol over fe-exchanged pillared beidellite," *Water research*, vol. 37, no. 5, pp. 1154–1160, 2003.

[74] L. A. Kaplan, "Comparison of high temperature and persulfate oxidation methods for determination of dissolved organic carbon in freshwaters," *Limnology and Oceanography*, vol. 37, no. 5, pp. 1119–1125, 1992.

[75] G. R. Peyton, "The free-radical chemistry of persulfate-based total organic carbon analyzers," *Marine Chemistry*, vol. 41, no. 1-3, pp. 91–103, 1993.

[76] National Center for Biotechnology Information, "Ammonium persulfate," 2017.

Appendices

Appendix A *Motor Step Sequences*

Enable = 0 for power to motor coil

Full Step

Step Sequence	Enable A	Phase A	Enable B	Phase B
0	0	1	0	0
1	0	0	0	0
2	0	0	0	1
3	0	1	0	1

Half Step

Step Sequence	Enable A	Phase A	Enable B	Phase B
0	0	1	0	0
1	1	0	0	0
2	0	0	0	0
3	0	0	1	1
4	0	0	0	1
5	1	1	0	1
6	0	1	0	1
7	0	1	1	0

Quarter Step

Step Sequence	Enable A	Phase A	Enable B	Phase B
0	0	1	0	0
1	0.5	1	0	0
2	1	0	0	0
3	0.5	0	0	0
4	0	0	0	0
5	0	0	0.5	0
6	0	0	1	1
7	0	0	0.5	1
8	0	0	0	1
9	0.5	0	0	1
10	1	1	0	1
11	0.5	1	0	1
12	0	1	0	1
13	0	1	0.5	1
14	0	1	1	0
15	0	1	0.5	0

Eighth Step

Step Sequence	Enable A	Phase A	Enable B	Phase B
0	0	1	0	0
1	0.25	1	0	0
2	0.5	1	0	0
3	0.75	1	0	0
4	1	0	0	0
5	0.75	0	0	0
6	0.5	0	0	0
7	0.25	0	0	0
8	0	0	0	0
9	0	0	0.25	0
10	0	0	0.5	0
11	0	0	0.75	0
12	0	0	1	1
13	0	0	0.75	1
14	0	0	0.5	1
15	0	0	0.25	1
16	0	0	0	1
17	0.25	0	0	1
18	0.5	0	0	1
19	0.75	0	0	1
20	1	1	0	1
21	0.75	1	0	1
22	0.5	1	0	1
23	0.25	1	1	1
24	0	1	0	1
25	0	1	0.25	1
26	0	1	0.5	1
27	0	1	0.75	1
28	0	1	1	0
29	0	1	0.75	0
30	0	1	0.5	0
31	0	1	0.25	0

Appendix B *Syringe Holder*

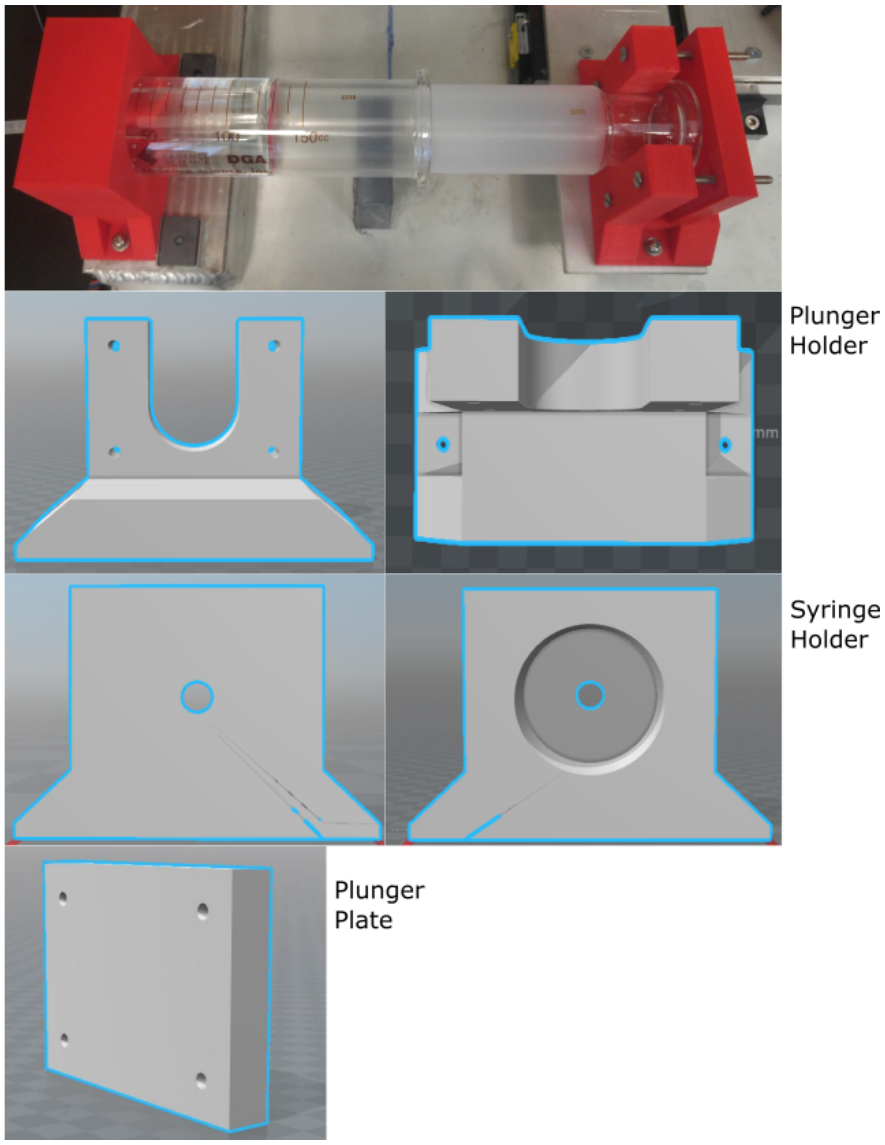

Appendix C *Arduino Code*

```
/*Stepper Motor and Temp Controller
  Max Liao
  University of Georgia
  Skidaway Institute of Oceanography
  Last update: 10-11-17
*/
//Libraries
#include "PlayingWithFusion_MAX31856.h"
#include "PlayingWithFusion_MAX31856_STRUCT.h"
#include "SPI.h"
#include "PID_v1.h"
//#include <PWM.h>

//Declare Variables

//PID
double aggkp = 12, aggki = 0, aggkd = 0;
double conkp = 12, conki = 0.5, conkd = 0;
double error;

//Frequencies
//int32_t frequency = 20000; //frequency (in Hz)

int SampleTime = 100;
  /*
  Thermocouple
     MOSI: pin 11  MOSI: pin 51  -->  SDI (must not be changed for hardware SPI)
     MISO: pin 12  MISO: pin 50  -->  SDO (must not be changed for hardware SPI)
     SCK:  pin 13  SCK:  pin 52  -->  SCLK (must not be changed for hardware SPI)*/

uint8_t TC0_CS  = 14;      // Analog Pin 0
uint8_t TC0_FAULT = 15;    // not used but needed for config setup
uint8_t TC0_DRDY  = 16;    // not used but needed for config setup

PWF_MAX31856  thermocouple0(TC0_CS, TC0_FAULT, TC0_DRDY);

static struct var_max31856 TC_CH0;
volatile double tmp, TCtmp;
struct var_max31856 *tc_ptr;

//Temperature PWM
const int TempPwmOut = 3;               // pin 3 will provide pwm output to the Heater
double TempPWM;                         // PWM value 0-255.
double Setpoint, SensorValue;

PID myPID(&SensorValue, &TempPWM, &Setpoint, conkp, conki, conkd, DIRECT);

//Pins
```

```
const int enableA = 5;           //blue (Wire color)
const int phaseA = 9;            //black
const int enableB = 6;           //red
const int phaseB = 10;           //yellow
const int plustravel = 4;        //white
const int minustravel = 7 ;      //blue
const int homepin = 8;           //green
const int brakepin = 2;

//Inputs
char command[10];
char inChar;
byte index = 0;
String COM;
int inData;
int stepmode = 0;
int stepmodemodifier;

//Motor Stepping
int dir = HIGH;                  //LOW = reverse (refill) , HIGH = forward (pump)
float stepspeed = 552;           //stepspeed*1 ms delay. 552 = 1 mL/min @ fullstep
//276 @ halfstep, 138 quarter, 79 eighth

double full = 127;               //50% duty cycle
double threeQ = 159;             //
double half = 191;               //
double quarter = 223;            //
bool limit, limitplus, limitminus, limithome;

void setup() {
  Serial.begin(115200);           // set baudrate of serial port
  Serial.println("Program Start");
  /* PWM frequency modifications
  //initialize all timers except for 0, to save time keeping functions
  InitTimersSafe();

  //sets the frequency for the specified pin
  bool successA = SetPinFrequencySafe(enableA, frequency);
  bool successB = SetPinFrequencySafe(enableB, frequency);

    Serial.print("Enable A: ");
    Serial.println(successA);
    Serial.print("Enable B: ");
    Serial.println(successB);

 */
  //set timer1 interrupt at 10Hz
  TCCR1A = 0;// set entire TCCR1A register to 0
  TCCR1B = 0;// same for TCCR1B
  TCNT1  = 0;//initialize counter value to 0
```

```
  // set compare match register for 10hz increments
  OCR1A = 6249;
  // = (16*10^6) / (10(interrupt frequency)*256(prescaler)) - 1 (must be <65536)

  // turn on CTC mode
  TCCR1B |= (1 << WGM12);
  // Set CS12 bit for 256 prescaler
  TCCR1B |= (1 << CS12);
  // enable timer compare interrupt
  TIMSK1 |= (1 << OCIE1A);

  // setup for the the SPI library:
  SPI.begin();                            // begin SPI
  SPI.setClockDivider(SPI_CLOCK_DIV16);   // SPI speed to SPI_CLOCK_DIV16 (1MHz)
  SPI.setDataMode(SPI_MODE3);             // MAX31856 is a MODE3 device

  // call config command...
  //options can be seen in the PlayingWithFusion_MAX31856.h file
  thermocouple0.MAX31856_config(T_TYPE, CUTOFF_60HZ, AVG_SEL_4SAMP, CMODE_AUTO);

  //Temperature PWM setup
  pinMode(TempPwmOut, OUTPUT);             //  Use pin 3 as Temperature PWM output

  //starting the PID
  Setpoint = 95;
  myPID.SetMode(AUTOMATIC);
  myPID.SetSampleTime(SampleTime);

  //Motor setup
  pinMode(phaseA, OUTPUT);
  pinMode(phaseB, OUTPUT);
  pinMode(enableA, OUTPUT);
  pinMode(enableB, OUTPUT);
  pinMode(plustravel, INPUT);
  pinMode(minustravel, INPUT);
  pinMode(homepin, INPUT);
  pinMode(brakepin, INPUT);
  brake(); //Make sure motor coils are off to start
}

void loop() {
  //Motor Stepping Input;
  while (Serial.available()) {
    input(); //Wait for user input
  }
}


//Interrupts
ISR(TIMER1_COMPA_vect) { //change the 1 to 0 for timer0 and 2 for timer2
```

```
// Read CH 0
tc_ptr = &TC_CH0;                              // set pointer
thermocouple0.MAX31856_update(tc_ptr);         // Update MAX31856 channel 0

if (TC_CH0.status)
{
  //lots of faults possible at once, tech
  //Faults detected can be masked,
  //please refer to library file to enable faults you want represented
  Serial.println("fault(s) detected");
  Serial.print("Fault List: ");
  if (0x01 & TC_CH0.status) {
    Serial.print("OPEN  ");
  }
  if (0x02 & TC_CH0.status) {
    Serial.print("Overvolt/Undervolt  ");
  }
  if (0x04 & TC_CH0.status) {
    Serial.print("TC Low  ");
  }
  if (0x08 & TC_CH0.status) {
    Serial.print("TC High  ");
  }
  if (0x10 & TC_CH0.status) {
    Serial.print("CJ Low  ");
  }
  if (0x20 & TC_CH0.status) {
    Serial.print("CJ High  ");
  }
  if (0x40 & TC_CH0.status) {
    Serial.print("TC Range  ");
  }
  if (0x80 & TC_CH0.status) {
    Serial.print("CJ Range  ");
  }
  Serial.println(" ");
}
else  // no fault, print temperature data
{
  // MAX31856 External (thermocouple) Temp
  TCtmp = (double)TC_CH0.lin_tc_temp * 0.0078125; // convert fixed pt# -> double
  Serial.print("TC temperature:");
  Serial.println(TCtmp);
  SensorValue = TCtmp;
  if (TCtmp) {
    if (TCtmp > 70  && TCtmp < 85) {
      //Serial.println("Set Aggresive Tunings");
      myPID.SetTunings(aggkp, aggki, aggkd);
    }
    else if (TCtmp > 85) {
```

```
        //Serial.println("Set Conservative Tunings");
        myPID.SetTunings(conkp, conki, conkd);
      }
    }
    myPID.Compute();
    if (TCtmp > 99)
    {
      TempPWM = 0;
    }
    else if (TCtmp < 70) {
      TempPWM = 255;
    }
    //Serial.print("PWM = ");
    float PWMpercent = TempPWM/255*100;
    //Serial.println(PWMpercent);
    analogWrite(TempPwmOut, TempPWM);
    //Serial.println(TempPWM);
  }
}


//User Input
int input() {
  while (Serial.available()) {
    COM = Serial.readString();
    Serial.println(COM);
    COM.toCharArray(command, 10);
  }
  if (COM.substring(0, 4) == "pump") {
    Serial.println("Pump Inputted");

    //Split pump input to get mL value based on deliminator ":"
    char delim[] = ":";
    char* volume = strtok(command, delim);
    int vol[] = {0, 0};

    while (volume != 0)
    {
      for (int i = 0; i < 2; i++)
      {
        vol[i] = atoi(volume);
        //Serial.println(vol[i]);
        volume = strtok(0, delim);
      }
      //Serial.println(vol[1]);
    }
    pump(vol[1], stepmode, stepspeed);
    index = clearinput(command);
    //return vol[1];
    //Serial.println(volume);
```

```
  return (1);
}
else if (COM.substring(0, 6) == "refill") {
  Serial.println("Refill Inputted");
  //Split refill input to get mL value based on deliminator ":"
  char delim[] = ":";
  char* volume = strtok(command, delim);
  int vol[] = {0, 0};

  while (volume != 0)
  {
    for (int i = 0; i < 2; i++)
    {
      vol[i] = atoi(volume);
      //Serial.println(vol[i]);
      volume = strtok(0, delim);
    }
    //Serial.println(vol[1]);
  }
  refill(vol[1], stepmode, stepspeed);
  index = clearinput(command);
  return (2);
}
else if (strcmp(command, "clear") == 0) {
  Serial.println("Cleared");
  brake();
  index = clearinput(command);
  return (3);
}
else if (strcmp(command, "full") == 0) {
  stepmode = 0;
  Serial.println("Full Step");
  index = clearinput(command);
  return (4);
}
else if (strcmp(command, "half") == 0) {
  stepmode = 1;
  Serial.println("Half Step");
  index = clearinput(command);
  return (5);
}
else if (strcmp(command, "quarter") == 0) {
  stepmode = 2;
  Serial.println("Quarter Step");
  index = clearinput(command);
  return (6);
}
else if (strcmp(command, "eighth") == 0) {
  stepmode = 2;
  Serial.println("Eighth Step");
```

```
    index = clearinput(command);
    return (7);
  }
  else if (strcmp(command, "rinse") == 0) {
    Serial.println("Rinsing");
    rinse();
    index = clearinput(command);
    return (8);
  }
  else if (strcmp(command, "empty") == 0) {
    Serial.println("Emptying");
    empty();
    index = clearinput(command);
    return (9);
  }
  else if (strcmp(command, "fill") == 0) {
    Serial.println("Filling");
    fill();
    index = clearinput(command);
    return (10);
  }
  else if (COM.substring(0, 4) == "flow") {
    Serial.println("Flow Inputted");
    //Split flow input to get mL/min value based on deliminator ":"
    char delim[] = ":";
    char* flow = strtok(command, delim);
    float fl[] = {0, 0};

    while (flow != 0)
    {
      for (int i = 0; i < 2; i++)
      {
        fl[i] = atof(flow);
        //Serial.println(vol[i]);
        flow = strtok(0, delim);
      }
      Serial.println(fl[1]);
    }
    stepspeed = flowrate(fl[1], stepmode);
    Serial.print("Stepspeed: ");
    Serial.println(stepspeed);
    index = clearinput(command);
    return (11);
  }
  else {
    index = clearinput(command);
    return (0);
  }
}
```

```
int clearinput(char* command) {
  for (int i = 0; i < 9; i++) {
    command[i] = 0;
  }
  return 0;
}


//Motor

//Motor Control with Limits
int limits(int dir, int stepspeed, int vol, int stepm)
//Pump/refill (High/Low) with limit controls
{
  Serial.println("Limits");
  limitplus = digitalRead(plustravel);
  limitminus = digitalRead(minustravel);
  limithome = digitalRead(homepin);
  if (dir == HIGH) {                    //If FORWARD
      if (stepm == 0) {
        fullstep(dir, stepspeed, vol); //Full stepping
      }
      else if (stepm == 1) {
        halfstep(dir, stepspeed, 0, vol); //Half stepping
      }
      else if (stepm == 2) {
        quarterstep(dir, stepspeed, 0, vol); //Quarter Stepping
      }
      else if (stepm == 3) {
        eighthstep(dir, stepspeed, 0, vol); //Eighth Stepping
      }
  }
  else if (dir == LOW) {
      if (stepm == 0) {
        fullstep(dir, stepspeed, vol); //Full stepping
      }
      else if (stepm == 1) {
        halfstep(dir, stepspeed, 0, vol); //Half stepping
      }
      else if (stepm == 2) {
        quarterstep(dir, stepspeed, 0, vol); //Quarter Stepping
      }
      else if (stepm == 3) {
        eighthstep(dir, stepspeed, 0, vol); //Eighth Stepping
      }
  }
  else {
    Serial.println("ER: Direction");
  }
}
```

```
void pump(int vol, int stepm, float stepspeed) {
  if (vol != 0) {
    Serial.println("Pumping:");
    Serial.print(vol);
    Serial.println(" mL");
    Serial.print("Stepmode: ");
    if (stepm == 0) {
      //stepspeed == 552;
      Serial.println("Full Step");
    }
    else if (stepm == 1) {
      //stepspeed =  276;
      Serial.println("Half step");
    }
    else if (stepm == 2) {
      //stepspeed = 138;
      Serial.println("Quarter step");
    }
    else if (stepm == 3) {
      //stepspeed = 79;
      Serial.println("Eighth step");
    }
    limits(HIGH, stepspeed, vol, stepm);
  }
  else if (vol > 150) {
    Serial.println("ER: Value Greater than 150");
  }
}

int refill(int vol, int stepm, float stepspeed)
{
  if (vol != 0) {
    Serial.println("Refilling:");
    Serial.print(vol);
    Serial.println(" mL");
    Serial.print("Stepmode: ");
    if (stepm == 0) {
      //stepspeed == 552;
      Serial.println("Full Step");
    }
    else if (stepm == 1) {
      //stepspeed = 276;
      Serial.println("Half step");
    }
    else if (stepm == 2) {
      //stepspeed = 138;
      Serial.println("Quarter step");
    }
    else if (stepm == 3) {
```

```
      //stepspeed = 69;
      Serial.println("Eighth step");
    }
    limits(LOW, stepspeed, vol, stepm);
  }
  else if (vol > 150) {
    Serial.println("ER: Value Greater than 150");
  }
}

void rinse()        //pump and refill syringe 3 times
{
  for (int i = 0; i < 3; i++)
  {
    limits(LOW, 10, 130, 0);
    if (limitminus == 1) {
      limits(HIGH, 10, 130, 0);
    }
  }
}

void fill()
{
  limits(LOW, 10, 150, 0);
}

void empty()
{
  limits(HIGH, 10, 150, 0);
}


//Motor Stepping Tables
void brake() {//All Off
  analogWrite(enableA, 255);
  analogWrite(enableB, 255);
  //digitalWrite(enableA, HIGH);
  //digitalWrite(enableB, HIGH);
}


void stepout(int seq, int stepspeed)
//Enable == 0 is coil on
{
  if (seq == 0)                     //Coil A = High, Coil B = High
  {
    digitalWrite(phaseA, HIGH);
    digitalWrite(phaseB, LOW);
    analogWrite(enableA, full);
    analogWrite(enableB, full);
```

```
}

else if (seq == 1)                  //Coil A = 3/4, Coil B = High
{
  digitalWrite(phaseA, HIGH);
  digitalWrite(phaseB, LOW);
  analogWrite(enableA, threeQ);    //75% on
  analogWrite(enableB, full);
}

else if (seq == 2)                  //Coil A = HALF, Coil B = HIGH
{
  digitalWrite(phaseA, HIGH);
  digitalWrite(phaseB, LOW);
  analogWrite(enableA, half);
  analogWrite(enableB, full);
}

else if (seq == 3)                  //Coil A = 1/4, Coil B = HIGH
{
  digitalWrite(phaseA, HIGH);
  digitalWrite(phaseB, LOW);
  analogWrite(enableA, quarter);     //25% on
  analogWrite(enableB, full);
}

else if (seq == 4)                  //Coil A = OFF, Coil B = HIGH
{
  digitalWrite(phaseA, LOW);        //PHASE A doesn't matter OFF
  digitalWrite(phaseB, LOW);
  analogWrite(enableA, HIGH);
  analogWrite(enableB, full);
}

else if (seq == 5)                  //Coil A = -1/4, Coil B = HIGH
{
  digitalWrite(phaseA, LOW);
  digitalWrite(phaseB, LOW);
  analogWrite(enableA, quarter);
  analogWrite(enableB, full);
}

else if (seq == 6)                  //Coil A = -HALF, Coil B = HIGH
{
  digitalWrite(phaseA, LOW);
  digitalWrite(phaseB, LOW);
  analogWrite(enableA, half);
  analogWrite(enableB, full);
}
```

```
else if (seq == 7)                  //Coil A = -3/4, Coil B = HIGH
{
  digitalWrite(phaseA, LOW);
  digitalWrite(phaseB, LOW);
  analogWrite(enableA, threeQ);
  analogWrite(enableB, full);
}

else if (seq == 8)                  //Coil A = LOW, Coil B = HIGH
{
  digitalWrite(phaseA, LOW);
  digitalWrite(phaseB, LOW);
  analogWrite(enableA, full);
  analogWrite(enableB, full);
}

else if (seq == 9)                  //Coil A = LOW, Coil B = 3/4
{
  digitalWrite(phaseA, LOW);
  digitalWrite(phaseB, LOW);
  analogWrite(enableA, full);
  analogWrite(enableB, threeQ);
}

else if (seq == 10)                  //Coil A = LOW, Coil B = HALF
{
  digitalWrite(phaseA, LOW);
  digitalWrite(phaseB, LOW);
  analogWrite(enableA, full);
  analogWrite(enableB, half);
}

else if (seq == 11)                  //Coil A = LOW, Coil B = 1/4
{
  digitalWrite(phaseA, LOW);
  digitalWrite(phaseB, LOW);
  analogWrite(enableA, full);
  analogWrite(enableB, quarter);
}

else if (seq == 12)                   //Coil A = LOW, Coil B = OFF
{
  digitalWrite(phaseA, LOW);
  digitalWrite(phaseB, HIGH);        //PHASE B doesn't matter OFF
  analogWrite(enableA, full);
  analogWrite(enableB, HIGH);
}

else if (seq == 13)                     //Coil A = LOW, Coil B = -1/4
{
```

```
  digitalWrite(phaseA, LOW);
  digitalWrite(phaseB, HIGH);
  analogWrite(enableA, full);
  analogWrite(enableB, quarter);
}

else if (seq == 14)                    //Coil A = LOW, Coil B = -HALF
{
  digitalWrite(phaseA, LOW);
  digitalWrite(phaseB, HIGH);
  analogWrite(enableA, full);
  analogWrite(enableB, half);
}

else if (seq == 15)                    //Coil A = LOW, Coil B = -3/4
{
  digitalWrite(phaseA, LOW);
  digitalWrite(phaseB, HIGH);
  analogWrite(enableA, full);
  analogWrite(enableB, threeQ);
}

else if (seq == 16)                    //Coil A = LOW, Coil B = LOW
{
  digitalWrite(phaseA, LOW);
  digitalWrite(phaseB, HIGH);
  analogWrite(enableA, full);
  analogWrite(enableB, full);
}

else if (seq == 17)                    //Coil A = -3/4, Coil B = LOW
{
  digitalWrite(phaseA, LOW);
  digitalWrite(phaseB, HIGH);
  analogWrite(enableA, threeQ);
  analogWrite(enableB, full);
}

else if (seq == 18)                    //Coil A = -HALF, Coil B = LOW
{
  digitalWrite(phaseA, LOW);
  digitalWrite(phaseB, HIGH);
  analogWrite(enableA, half);
  analogWrite(enableB, full);
}

else if (seq == 19)                    //Coil A = -1/4, Coil B = LOW
{
  digitalWrite(phaseA, LOW);
  digitalWrite(phaseB, HIGH);
```

```
  analogWrite(enableA, quarter);
  analogWrite(enableB, full);
}

else if (seq == 20)                  //Coil A = OFF, Coil B = LOW
{
  digitalWrite(phaseA, HIGH);        //PHASE A doesn't matter OFF
  digitalWrite(phaseB, HIGH);
  analogWrite(enableA, HIGH);
  analogWrite(enableB, full);
}

else if (seq == 21)                   //Coil A = quarter, Coil B = LOW
{
  digitalWrite(phaseA, HIGH);
  digitalWrite(phaseB, HIGH);
  analogWrite(enableA, quarter);
  analogWrite(enableB, full);
}

else if (seq == 22)                  //Coil A = HALF, Coil B = LOW
{
  digitalWrite(phaseA, HIGH);
  digitalWrite(phaseB, HIGH);
  analogWrite(enableA, half);
  analogWrite(enableB, full);
}

else if (seq == 23)                  //Coil A = 3/4, Coil B = LOW
{
  digitalWrite(phaseA, HIGH);
  digitalWrite(phaseB, HIGH);
  analogWrite(enableA, threeQ);
  analogWrite(enableB, full);
}

else if (seq == 24)                  //Coil A = HIGH, Coil B = LOW
{
  digitalWrite(phaseA, HIGH);
  digitalWrite(phaseB, HIGH);
  analogWrite(enableA, full);
  analogWrite(enableB, full);
}

else if (seq == 25)                  //Coil A = HIGH, Coil B = -3/4
{
  digitalWrite(phaseA, HIGH);
  digitalWrite(phaseB, HIGH);
  analogWrite(enableA, full);
  analogWrite(enableB, threeQ);
```

```
}

else if (seq == 26)                   //Coil A = HIGH, Coil B = -HALF
{
  digitalWrite(phaseA, HIGH);
  digitalWrite(phaseB, HIGH);
  analogWrite(enableA, full);
  analogWrite(enableB, half);
}

else if (seq == 27)                   //Coil A = HIGH, Coil B = -1/4
{
  digitalWrite(phaseA, HIGH);
  digitalWrite(phaseB, HIGH);
  analogWrite(enableA, full);
  analogWrite(enableB, quarter);
}

else if (seq == 28)                   //Coil A = HIGH, Coil B = OFF
{
  digitalWrite(phaseA, HIGH);
  digitalWrite(phaseB, LOW);          //PHASE B doesn't matter OFF
  analogWrite(enableA, full);
  analogWrite(enableB, HIGH);
}

else if (seq == 29)                   //Coil A = HIGH, Coil B = 1/4
{
  digitalWrite(phaseA, HIGH);
  digitalWrite(phaseB, LOW);
  analogWrite(enableA, full);
  analogWrite(enableB, quarter);
}

else if (seq == 30)                   //Coil A = HIGH, Coil B = HALF
{
  digitalWrite(phaseA, HIGH);
  digitalWrite(phaseB, LOW);
  analogWrite(enableA, full);
  analogWrite(enableB, half);
}

else if (seq == 31)                   //Coil A = HIGH, Coil B = 3/4
{
  digitalWrite(phaseA, HIGH);
  digitalWrite(phaseB, LOW);
  analogWrite(enableA, full);
  analogWrite(enableB, threeQ);
}
else {
```

```
    Serial.println("ER: Step Sequence");
  }

  delay(stepspeed);                     //Time between steps = stepspeed
}


//Stepping Modes

/*Syringe volume = 150 mL = 150000 mm^3.
Syringe ID = 42.95 mm -> Surface area = (ID/2)^2*pi = 1448.8 mm^2.
Syringe length for 150mL = Syringe volume/Surface area = 103.5321 mm.
Travel per full step = 0.00025 inches = 0.00635.
Full steps for 150 mL = Syringe Length/travel per full step = 1.6304*10^4
mL per full step = 150/Full steps for 150mL = 0.0092 mL/Full Step.
Steps in fullstep sequence = 4
Full steps for 1 mL = 1/(mL per full step) = 108.6951
Full step delay for 1mL/min = 60,000 ms /(Full steps for 1 mL)= 552 ms
mL per full step * full step sequence = 0.0368 mL per step sequence
*/

float flowrate(float flowr, int stepm){
  if (stepm ==0){stepmodemodifier = 1;}        //Full step
  else if(stepm ==1){stepmodemodifier = 2;}    //half step
  else if(stepm ==2){stepmodemodifier = 4;}    //quarter step
  else if(stepm ==3){stepmodemodifier = 8;}    //eighth step
  float base = 552;
  stepspeed = (base/flowr)/stepmodemodifier;    //1 mL/min stepspeed = 552ms
  return stepspeed;
}

void fullstep(int dir, int stepspeed, int vol) {
  Serial.println("Full Stepping");
  float volume = float(vol);
  //Serial.println(volume);
  float steps = (vol / 0.0368);
  //Serial.println(steps);
  float stepsint = round(steps);
  //Serial.println(stepsint);
  if (dir == HIGH) {
    for (int i = 0; i < stepsint; i++) {      //Loop for a full step sequence
      limitminus = digitalRead(minustravel);
      if (limitminus ==1){                    //Stops if linear stage limit reached
        Serial.println("Minus High");
        break;
      }
      else if (i == stepsint - 1) {
        Serial.println("Done Full Stepping");
        break;
      }
```

```
      //Serial.println(i);
      fullforward(stepspeed);
      //Serial.print("full stepping forward \n");
    }
    brake();
   }
  else {
    for (int i = 0; i < stepsint; i++) {
      limitplus = digitalRead(plustravel);
      if (limitplus ==1){
        Serial.println("Plus High");
        break;
      }
      else if (i == stepsint - 1) {
        Serial.println("Done Full Stepping");
        break;
      }
     //Serial.println(i);
     fullreverse(stepspeed);
    }
    brake();
    //Serial.print("full stepping reverse \n");
  }
}

void fullforward(int stepspeed) {
  stepout(0, stepspeed);
  stepout(8, stepspeed);
  stepout(16, stepspeed);
  stepout(24, stepspeed);
}

void fullreverse(int stepspeed) {
  stepout(24, stepspeed);
  stepout(16, stepspeed);
  stepout(8, stepspeed);
  stepout(0, stepspeed);
}

void halfstep(int dir, int stepspeed, int seq, int vol) {
  float volume = float(vol);
  //Serial.println(volume);
  float steps = (vol / 0.0368);
  //Serial.println(steps);
  float stepsint = round(steps);
  for (int i = 0; i < stepsint; i++) {
    limitminus = digitalRead(minustravel);
      if (limitminus ==1){
        Serial.println("Minus High");
        break;
```

```
      }
      else if (i == stepsint - 1) {
      Serial.println("Done Half Stepping");
      break;
    }
     //Serial.println(i);
    //Serial.print("half stepping forward \n");
    for (int x = 0; x < 8; x++) {
      if (dir == HIGH && seq < 28) {
        seq = seq + 4;
      }
      else if (dir == HIGH && seq == 28) {
        seq = 0;
      }
      else if (dir == LOW && seq > 0) {
        seq = seq - 4;
      }
      else if (dir == LOW && seq == 0) {
        seq = 28;
      }
      else(Serial.println("ER: Half stepping"));
      stepout(seq, stepspeed);
    }
  }
  brake();
}

void quarterstep(int dir, int stepspeed, int seq, int vol) {
  float volume = float(vol);
  //Serial.println(volume);
  float steps = (vol / 0.0368);
  //Serial.println(steps);
  float stepsint = round(steps);
  for (int i = 0; i < stepsint; i++) {
      limitminus = digitalRead(minustravel);
      if (limitminus ==1){
        Serial.println("Minus High");
        break;
      }
      else if (i == stepsint - 1) {
      Serial.println("Done Quarter stepping");
    }
    //Serial.println(i);
    //Serial.print("micro stepping forward \n");
    for (int x = 0; x < 16; x++) {
      if (dir == HIGH && seq < 30) {
        seq = seq + 2;
      }
      else if (dir == HIGH && seq == 30) {
        seq = 0;
```

```
      }
      else if (dir == LOW && seq > 0) {
        seq = seq - 2;
      }
      else if (dir == LOW && seq == 0) {
        seq = 30;
      }
      else(Serial.println("ER: Quarter stepping"));
      stepout(seq, stepspeed);
    }
  }
}

void eighthstep(int dir, int stepspeed, int seq, int vol) {
  float volume = float(vol);
  //Serial.println(volume);
  float steps = (vol / 0.0368);
  //Serial.println(steps);
  float stepsint = round(steps);
  for (int i = 0; i < stepsint; i++) {
      limitminus = digitalRead(minustravel);
      if (limitminus ==1){
        Serial.println("Minus High");
        break;
      }
      else if (i == stepsint - 1) {
      Serial.println("Done Eighth stepping");
    }
    //Serial.println(i);
    //Serial.print("micro stepping forward \n");
    for (int x = 0; x < 32; x++) {
      if (dir == HIGH && seq < 31) {
        seq = seq + 1;
      }
      else if (dir == HIGH && seq == 31) {
        seq = 0;
      }
      else if (dir == LOW && seq > 0) {
        seq = seq - 1;
      }
      else if (dir == LOW && seq == 0) {
        seq = 31;
      }
      else(Serial.println("ER: Eighth stepping"));
      stepout(seq, stepspeed);
    }
  }
}
```

Appendix D *Arduino Wiring Diagram*

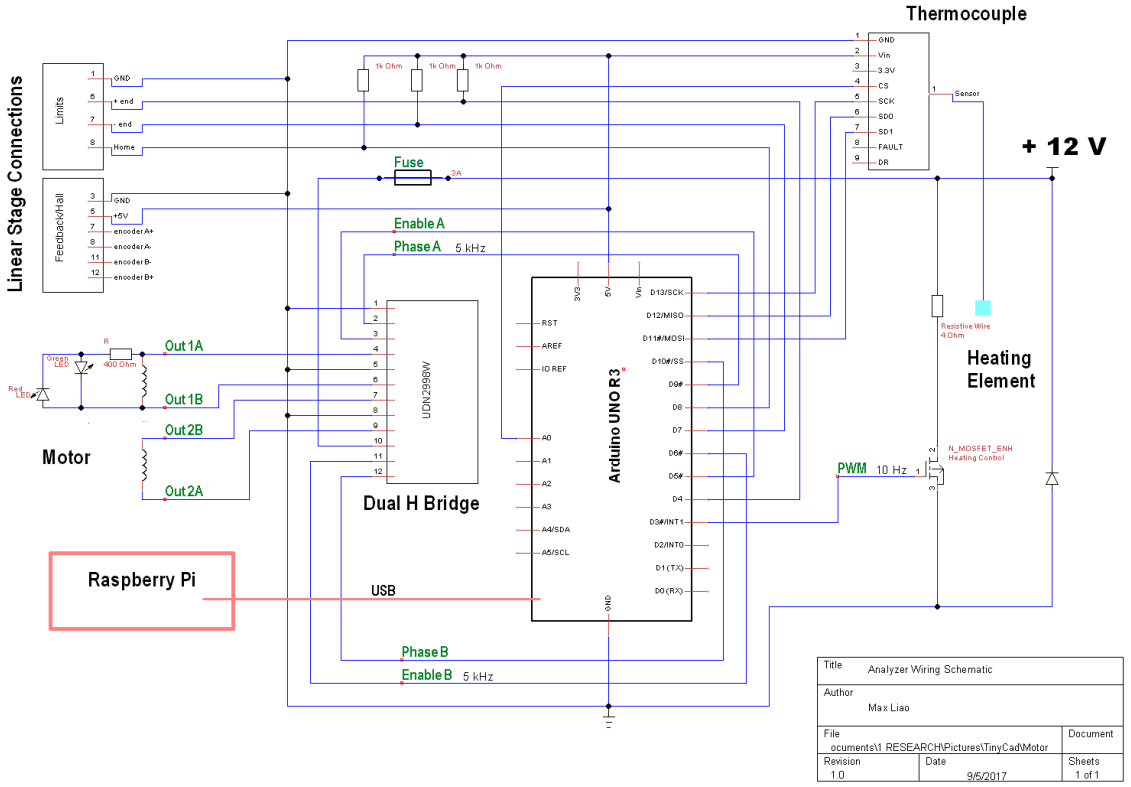

Appendix E ***Extraction Efficiency Matlab Code***

```
function ppm = Concentrationppm(liqflowrate,gasflowrate,temperature,pressure,H2Ovapor)

mNaCO3 = .212; %g/L
mwNaCO3 = 106; %Molar weight
mwCO2 = 44;    %Molar weight CO2

MNaCO3 = mNaCO3/mwNaCO3; %number of moles NaCO3 = moles C = mass/mw (Moles C/L)
liqL = liqflowrate/1000; %mL to L
gasL = gasflowrate/1000; %mL to L
MliqC = MNaCO3*liqL; %moles C/L *L/min
MgasC = MliqC/gasL; %moles C/L in gas

liqCO2 = MNaCO3*mwCO2; %grams of CO2 per liter water = moleC * MWCO2
gasCO2 = MgasC*mwCO2;  %grams of CO2 per liter air

MWgas = 28.975;
temp = temperature + 273.15; %
R = 0.082057338; %Ideal Gas Constant L*atm/(K*mol)

PAVol = 1; %per L gas
patm = pressure/98.6923;
n =(patm*PAVol)/(R*temp); %moles zerograde per L
ggas = n*MWgas; %g = moles *g/moles

H2Ov = H2Ovapor/1000;   %um/m of H2O in gas stream
gH2O = (H2Ov*(gasCO2 + ggas))/(1-H2Ov); %grams of H2O =
partsper = gasCO2/(gasCO2+ggas+gH2O); %Concentration
ppm = partsper * 1000000; %ppm
end
```